Studies of Spin-Orbit Correlations in Kaon Electroproduction in DIS with polarized hydrogen and deuterium targets

H. Avakian[†*], A. Bacchetta, V.D. Burkert, L.Elouadrhiri, V. Kubarovsky, S Stepanyan
Jefferson Lab, Newport News, VA 23606, USA

E. Cisbani[†], F. Cusanno, F. Garibaldi, S. Frullani
INFN Roma I and Istituto Superiore di Sanita', I-00161 Rome, Italy

P. Rossi[†], E. De Sanctis, L. Hovsepyan, M. Mirazita, and S. Anefalos Pereira
INFN, Laboratori Nazionali di Frascati , Via E. Fermi, I-00044 Frascati, Italy

K. Hafidi[†], J. Arrington, P. Dupré, D. F. Geesaman, R. J. Holt,
D. H. Potterveld, P. E. Reimer, P. Solvignon
Argonne National Lab, Argonne, IL 60439, USA

K. Griffioen[†], Bo Zhao
College of William & Mary, VA 23187, USA

M. Aghasyan, S.E. Kuhn Old Dominion University, Norfolk, VA 23529, USA

Z.-E. Meziani, B. Sawatzky, A. Lukhanin
Temple University 1900 N. 13th St.Philadelphia, PA 19122, 6082, USA

D. Ireland, R. Kaiser, K. Livingston, D. MacGregor, G. Rosner, B. Seitz[†]
Univ. of Glasgow, Glasgow G12 8QQ, UK

K. Joo, P. Schweitzer, M. Ungaro
University of Connecticut, Storrs, CT 06269, USA

P.F. Dalpiaz, G. Ciullo, M. Contalbrigo, F. Giordano, P. Lenisa, L. Pappalardo
University of Ferrara, Via Paradiso, I-44100, Ferrara, Italy

A. D'Angelo, C. Schaerf, V. Vegna
INFN Sezione di Roma Tor Vergata, Via della Ricerca Scientifica 1- I00133, Rome, Italy

R. De Leo, L. Lagamba, S. Marrone, G. Simonetti, E. Nappi, I. Vilardi
INFN Sezione di Bari and University of Bari, 70126 Bari, Italy

G.M. Urciuoli , INFN Roma I, I-00161 Rome, Italy

M. Battaglieri, R. De Vita, V. Drozdov, M. Osipenko, M. Ripani, M. Taiuti
Dipartamento di Fisica and INFN, Sezione di Genova, Via Dodecaneso, 33 I-16146 Genova, Italy

V. Bellini, A. Giusa, F. Mammoliti, C. Randieri, G. Russo, M.L. Sperduto, C.M. Sutera
INFN - Sezione di Catania and Universita' di Catania, I-95123 Catania, Italy

N. Kalantarians, D. Crabb, L.C. Smith, UVA, Charlottesville, VA 22904,USA

R. Avagyan, A. Avetisyan, R. Dallakyan, S. Taroyan

Yerevan Physics Institute, Alikhanian Br. 2, Yerevan, Armenia

F. Benmokhtar, Carnegie Mellon University, 5000 Forbes Avenue, Pittburgh, PA 15213, USA

M. Anselmino, A. Kotzinian, B. Parsamyan, A. Prokudin
Università di Torino and INFN, Sezione di Torino, Via P. Giuria 1, I-10125 Torino
M. Burkardt, New Mexico State University, PO Box 30001, Las Cruces, NM 88003, USA
B. Pasquini, Universita degli Studi di Pavia, Pavia, Italy
L. Gamberg, Penn State Berks, Reading, PA 19610, USA
G.R. Goldstein, Tufts University, Medford, MA 02155, USA

A CLAS collaboration proposal

† Co-spokesperson * Contact: Harut Avakian, JLab, Newport News VA 23606. Email: avakian@jlab.org

Collaborators' commitment to the 12 GeV upgrade of Jefferson Lab

- **Italian JLAB12 collaboration**

  The Italian JLAB12 collaboration (INFN Bari, INFN Catania, Laboratori Nazionali di Frascati, INFN Genova, INFN Roma I and Istituto Superiore di Sanita', INFN Roma Tor Vergata) is actively involved in this proposal. Among CLAS12 equipment, the group plans to contribute to the design, prototyping, construction and testing of the CLAS12 RICH detector and central calorimeter. Seven staff members and three post-docs will spend their time as needed on this project. Funding for the group is from the Italian research agency Istituto Nazionale di Fisica Nucleare (INFN). Additional funding are planned to be sought in the European Community.

- The College of William and Mary group is actively involved in this proposal, as well as several other proposals using CLAS12. Other members of our group are also pursuing a proposal for Hall A, but their contributions are not included here. Among CLAS12 baseline equipment, the group is committed to building part of the forward tracking system, but the exact tasks have not yet been determined. At least one faculty member, two graduate students, half a post-doc and several undergraduates are likely to work at least part time on this project in the next few years. Funding for the group is from the DOE and from the NSF. Additional funding will be sought for building the base equipment. Facilities at William and Mary include a clean room suitable for drift-chamber construction, and, on the time scale of a few years in the future, ample space for detector construction and testing.

- Argonne National Laboratory Medium Energy group is actively involved in this proposal, as well as other proposals using CLAS12. Among CLAS12 baseline equipment, the group intends to take responsibility for the design, prototyping, construction and testing of the high threshold Cerenkov counter. 3 research staff and 2 engineers are likely to work at least part time on this project in the next few years. Funding for the group is from DOE. Additional sources of funding will be sought as appropriate. Beyond the baseline equipment, the group is also interested in exploring the possibility of building a RICH detector for CLAS12.

Abstract

We are proposing a comprehensive program to study transverse momentum dependence of valence quark transverse and longitudinal spin distributions through measurements of spin-azimuthal asymmetries in semi-inclusive electroproduction of kaons using the upgraded JLab 11 GeV polarized electron beam and the CLAS12 detector with longitudinally polarized proton and deuteron targets. Main objectives include studies of correlations of the transverse spin of quarks with their transverse momentum, leading to observable spin and azimuthal asymmetries. The measurement of the $\sin 2\phi$ azimuthal moment of the semi-inclusive production of hadrons in DIS with longitudinally polarized targets, in particular will provide direct information on spin-orbit correlations by measuring the leading twist transverse momentum dependent (TMD) parton distributions related to the interference between states with different orbital momenta. Measurements with kaons are complementary to measurements with pions and will provide additional information on the Collins fragmentation mechanism. The P_T dependence of the double spin asymmetry will provide additional information on the flavor and polarization dependence of transverse momentum dependence of helicity distributions of quarks, providing complementary to SSA measurements access to spin-orbit correlations. The x, z, P_T and Q^2 dependences of the $\sin 2\phi$ and $\sin \phi$ moments will be studied to probe the underlying T-odd distribution and fragmentation functions. The experiment will use the upgraded CLAS12 detector, 11 GeV highly polarized electron beam and longitudinally polarized solid ammonia targets (NH_3 and ND_3). Kaon identification in the complete kinematic range will be done by the proposed CLAS12-RICH proximity-focusing detector. The large acceptance of CLAS12 would allow simultaneous detection of the scattered electrons and leading hadrons from the hadronization of the struck quark, providing information on its flavor and transverse momentum. We request 30 days of running on NH_3 and 50 days of running on ND_3 (or possibly ^{6}Li D or HD), including about 20% overhead for target anneals, polarization reversal, and auxiliary measurements. This measurement will simultaneously run with already appro ved measurements using pion electroproduction.

Contents

1 Introduction

Semi-inclusive deep inelastic scattering (SIDIS) has been used extensively in recent years as an important testing ground for QCD. Studies so far have concentrated on better determination of parton distribution functions, distinguishing between the quark and antiquark contributions, and understanding the fragmentation of quarks into hadrons. The use of polarization in leptoproduction provides an essential new dimension for testing QCD. The spin structure of the nucleon has been of particular interest since the EMC [1] measurements implied that the helicity of the constituent quarks account for only a fraction of the nucleon spin. Possible interpretations of the small fraction of the spin carried by quark helicities include the contribution of the orbital momentum of quarks and gluons and significant polarization of either the strange sea (negatively polarized) or gluons (positively polarized).

Azimuthal distributions of final state particles in semi-inclusive deep inelastic scattering are sensitive to the orbital motion of quarks and play an important role in the study of transverse momentum distributions of quarks in the nucleon. Correlations of spin and transverse momentum of quarks are by now universally recognized as essential ingredients of the structure of hadrons. They are described by a number of Transverse Momentum dependent Distribution functions (TMDs) [2, 3] which give rise to various observables in hard hadronic processes [4].

Large Single Spin Asymmetries (SSAs), have been among the most difficult phenomena to understand from first principles in QCD and can be also related to TMDs. Two fundamental mechanisms have been identified leading to SSAs in hard processes; the Sivers mechanism [5, 6, 7, 8, 9], which generates an asymmetry in the distribution of quarks due to orbital motion of partons, and the Collins mechanism [8, 2], which generates an asymmetry during the hadronization of quarks.

Significant progress has been made recently in understanding the role of partonic initial and final state interactions [7, 8, 9]. The interaction between the active parton in the hadron and the spectators was included in gauge-invariant TMD distributions [7, 8, 9, 10, 11]. Furthermore, QCD factorization for semi-inclusive deep inelastic scattering at low transverse momentum in the current-fragmentation region has been established in Refs. [12, 13]. This new framework provides a rigorous basis to study the TMD parton distributions from SIDIS data using different spin-dependent and independent observables. TMD distributions (see Table 1) describe transitions of a nucleon with one polarization in the initial state to a quark with another polarization in the final state.

The diagonal elements of the table are the momentum, longitudinal and transverse spin distributions of partons, and represent well-known parton distribution functions related to the square of the leading-twist, light-cone wave functions. Off-diagonal elements require non-zero orbital angular momentum and are related to the overlap of light-cone wave functions with $\Delta L \neq 0$ [14]. The parton distributions $f_{1T}^{\perp}$ and $h_1^{\perp}$ represent the imaginary parts of the corresponding interference terms, while the functions g_{1T} and $h_{1L}^{\perp}$ represent their real parts. The TMDs $f_{1T}^{\perp}$ (chiral-even) and $h_1^{\perp}$ (chiral-odd) are known as the Sivers and Boer-Mulders functions, respectively [5, 6, 15, 8, 9, 10]. They describe unpolarized quarks in the transversely polarized nucleon and transversely polarized quarks in the unpolarized nucleon respectively. They vanish at tree-level in a T-reversal invariant model (T-odd) and can only be non-zero when initial or final state interactions cause an interference between

N \ q	U	L	T
U	$\mathbf{f_1}$		$h_1^\perp$
L		$\mathbf{g_1}$	$h_{1L}^\perp$
T	$f_{1T}^\perp$	g_{1T}	$\mathbf{h_1}$ $h_{1T}^\perp$

Table 1: Leading-twist transverse momentum-dependent distribution functions. U, L, and T stand for transitions of unpolarized, longitudinally polarized, and transversely polarized nucleons (rows) to corresponding quarks (columns).

different helicity states. These functions parametrize the correlation between the transverse momentum of quarks and the spin of a transversely polarized target or the transverse spin of the quark, respectively. They require both orbital angular momentum, as well as non-trivial phases from the final state interaction, that survive in the Bjorken limit. The T-even counterpart of the Boer-Mulders function, $h_{1L}^\perp$, first introduced by Ralston and Soper [16], describes the correlations of the transverse spin of quarks in the longitudinally polarized nucleon and their transverse momentum.

Parton distribution and fragmentation functions in DIS, Drell-Yan and electron-positron annihilation have different gauge links, which raised a question of the universality of those functions [13, 11, 17]. It has been found that all six T-even TMD parton distributions are the same in SIDIS and Drell-Yan. The violation of universality for T-odd distributions appeared to be just a sign reverse from DIS to Drell-Yan, an exciting prediction that has to be confirmed by future experiments. Universality of TMDs in processes with hadrons in both initial and final states is violated, at least in its standard form [18, 17, 19], with far-reaching consequences in hadron colliders physics.

Similar correlations arise in the hadronization process. One particular case is the Collins T-odd fragmentation function $H_1^\perp$ [20] describing fragmentation of transversely polarized quarks into unpolarized hadrons. The Collins function is one of the most fundamental quantities accessible in hard fragmentation processes. It is of essential importance for spin physics because it works as an analyzer of the spin of the quark, but it is also interesting on its own because it allows the exploration of spin and orbital degrees of freedom of the QCD vacuum. It is universal [21, 13, 22], once measured in e^+e^-, it can be used in SIDIS and pp collisions and vice versa. For kaons in particular, the u to kaons Collins fragmentation function allows for exploring the structure of the strange vacuum, while the s to kaons Collins function allows for study the spin structure of the strangeness in the nucleon.

In recent years, measurements of azimuthal moments of hadronic cross sections in hard processes have emerged as a powerful tool to probe nucleon structure through transverse single spin asymmetries. Many experiments worldwide are currently trying to pin down various TMD effects through semi-inclusive deep-inelastic scattering (in experiments such as HERMES at DESY [23, 24, 25, 26], COMPASS at CERN [27], CLAS and Hall-A at Jefferson Lab [28, 29]) polarized proton-proton collisions (PHENIX, STAR and BRAHMS at RHIC) [30, 31, 32], and electron-positron annihilation (Belle at KEK) [33]. In contrast to inclusive deep inelastic lepton-nucleon scattering where transverse momentum is integrated out, these processes are sensitive to transverse momentum scales on the order of the intrinsic quark

momentum $P_T \sim k_\perp$.

Orbital momentum of quarks may also significantly change the helicity distribution of quarks in the valence quark region, in particular the distributions of quarks anti-aligned with proton spin [34, 35]. Simple model calculations also indicate that quark distributions aligned, q^+, and anti-aligned, q^-, with proton spin will have also very different transverse momentum distributions [36]. That may lead to observable effects in transverse momentum, P_T, dependences of double-spin longitudinal asymmetries [37]. Correlations of transverse spin of quarks in the longitudinally polarized nucleons and their transverse momentum also lead to observable Single Spin Asymmetries (SSAs)[2, 38].

The JLab 12-GeV upgrade will provide the unique combination of wide kinematic coverage, high beam intensity (luminosity), high energy, high polarization, and advanced detection capabilities necessary to study the transverse momentum and spin correlations in double-polarized semi-inclusive processes both in the target and current fragmentation regions for variety of hadron species. Measurements of spin-orbital structure of hadrons with longitudinally polarized targets were approved in case of pions [39]. In this proposal we focus on observables related to kaon production in DIS, accessible with longitudinally polarized targets and new information on the structure of nucleon they can provide.

1.1 Spin and Azimuthal Asymmetries in SIDIS

The SIDIS cross section at leading twist has eight contributions related to different combinations of the polarization state of the incoming lepton and the target nucleon [40, 2, 12, 3]. The lepton-hadron cross section can then be parametrized as [3]

$$
\begin{aligned}
\frac{d\sigma}{dx\,dy\,dz\,d\phi_S\,d\phi_h\,dP_{h\perp}^2} &= \frac{\alpha^2}{xQ^2}\,\frac{y}{2\,(1-\varepsilon)} \\
&\times \Bigg\{ F_{UU,T} + \varepsilon\cos(2\phi_h)\,F_{UU}^{\cos 2\phi_h} + S_L\,\varepsilon\sin(2\phi_h)\,F_{UL}^{\sin 2\phi_h} \\
&\quad + S_L\lambda_e\sqrt{1-\varepsilon^2}\,F_{LL} + |\boldsymbol{S}_T|\,\Bigg[\sin(\phi_h-\phi_S)\,F_{UT,T}^{\sin(\phi_h-\phi_S)} \\
&\qquad + \varepsilon\,\sin(\phi_h+\phi_S)\,F_{UT}^{\sin(\phi_h+\phi_S)} + \varepsilon\,\sin(3\phi_h-\phi_S)\,F_{UT}^{\sin(3\phi_h-\phi_S)}\Bigg] \\
&\quad + |\boldsymbol{S}_T|\,\lambda_e\left[\sqrt{1-\varepsilon^2}\,\cos(\phi_h-\phi_S)\,F_{LT}^{\cos(\phi_h-\phi_S)}\right]\Bigg\}\,,
\end{aligned}
\tag{1}
$$

where α is the fine structure constant and ε the ratio of longitudinal and transverse photon flux,

$$
\varepsilon = \frac{1-y}{1-y+y^2/2}\,. \tag{2}
$$

The kinematic variables x, y are defined as: $x = Q^2/2(P_1q)$, and $y = (P_1q)/(P_1k_1)$. The variable $q = k_1 - k_2$ is the momentum of the virtual photon, $Q^2 = -q^2$, ϕ_h is the azimuthal angle between the scattering plane formed by the initial and final momenta of the electron and the production plane formed by the transverse momentum of the observed hadron and the virtual photon (see Fig. 1), and ϕ_S is the azimuthal angle of the transverse spin in

the scattering plane. The subscripts in F_{UL}, F_{LL},etc., specify the beam (first index) and target(second index) polarizations, longitudinal (L), transverse (T), and unpolarized (U).

Structure functions factorize into TMD parton distributions, fragmentation functions, and hard parts [12, 3]

$$\begin{aligned} \sigma_{UU} \propto F_{UU} \propto & \quad f_1(x,k_\perp)\, D_1(z_h,p_\perp)\, H_{UU}(Q^2) \\ \sigma_{LL} \propto F_{LL} \propto & \quad g_{1L}(x,k_\perp)\, D_1(z_h,p_\perp)\, H_{LL}(Q^2) \\ \sigma_{UL} \propto F_{UL} \propto & \quad h_{1L}^\perp(x,k_\perp)\, H_1^\perp(z_h,p_\perp)\, H_{UL}(Q^2), \end{aligned} \tag{3}$$

where $z = (P_1 P_h)/(P_1 q)$, $k_\perp$ and $p_\perp$ are quark transverse momenta before and after scattering, and P_1 and P_h are the four momenta of the initial nucleon and the observed final-state hadron respectively.

The unpolarized D_1 and polarized $H_1^\perp$ fragmentation functions depend in general on the transverse momentum of the fragmenting quark.

S_L and S_T are longitudinal and transverse components of the target polarization with respect to the direction of the virtual photon. The different hard factors (H_{UU}, H_{LL},etc.), which are calculable in pQCD, in the SIDIS cross section are similar at one-loop order [12] and may cancel to a large extent in asymmetry observables.

In the case of the polarized beam and unpolarized or longitudinally polarized target the cross section in the leading order has only two contributions that depend on the azimuthal angle of the final state hadron, appearing as $\cos 2\phi$ and $\sin 2\phi$ modulations, involving four leading twist TMD distribution functions [2, 41, 40].

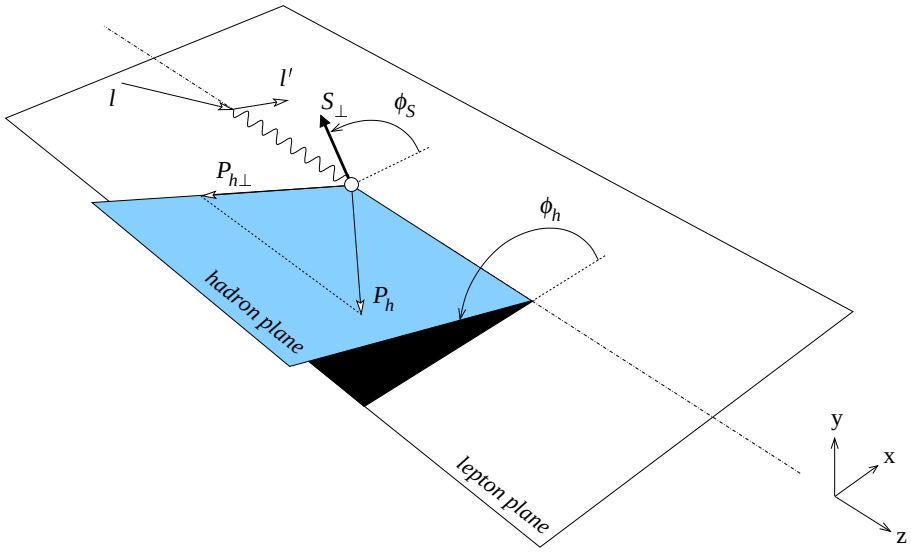

Figure 1: SIDIS kinematics. For a longitudinally polarized target, ϕ_S=0 or 180^o for negative and positive helicities of the proton, respectively.

During the last few years, first results on transverse SSAs have become available [25, 27]. Pioneering measurements by the HERMES Collaboration for the first time directly indicated significant azimuthal moments generated both by Collins ($F_{UT}^{\sin(\phi+\phi_S)}$) and Sivers ($F_{UT}^{\sin(\phi-\phi_S)}$)

effects. Significant differences were observed between charged pion and kaon, both for Sivers and Collins effects (see Fig.2). Currently no satisfactory explanation exists for these observed differences.

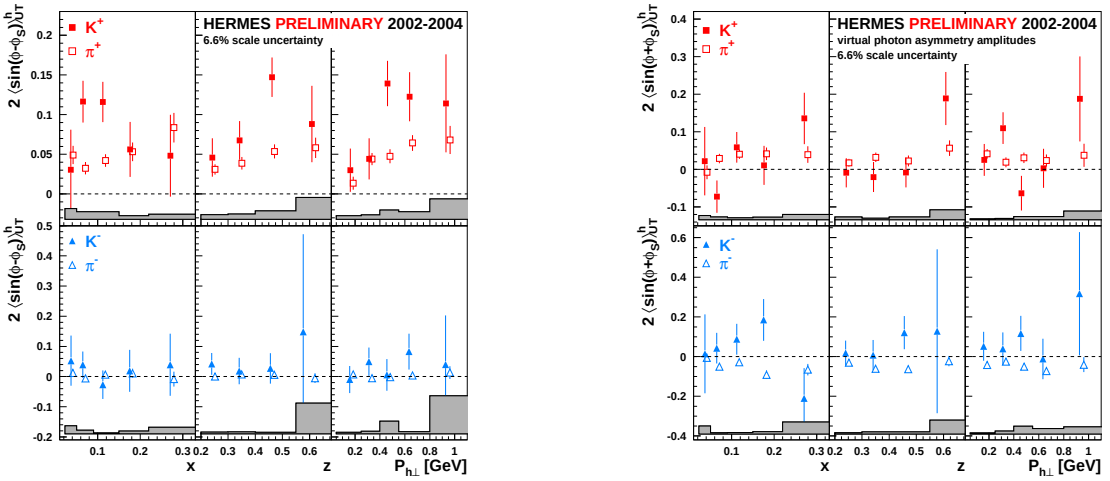

Figure 2: First measurements of Collins (right) and Sivers(left) asymmetries for pions and kaons.

1.1.1 Azimuthal Asymmetries in longitudinally polarized SIDIS

In the collinear limit of QCD, integrating over the transverse momentum, integrated ($f_1^a(x) = \int \mathrm{d}^2\mathbf{p}_T f_1(x,\mathbf{p}_T)$) and FFs ($D_1^a(z) = \int \mathrm{d}^2\mathbf{K}_T D_1(z,\mathbf{K}_T)$) remain, so the azimuthal dependences due to correlations of transverse momentum of partons and their spin vanish.

Spin-orbit correlations are accessible in SIDIS with longitudinally polarized target in measurements of double and single-spin asymmetries. For a longitudinally polarized target the only azimuthal asymmetry arising in leading order is the $\sin 2\phi$ moment,

$$\sigma_{UL}^{\sin 2\phi} \propto S_L 2(1-y)\sin 2\phi \sum_{q,\bar{q}} e_q^2 x h_{1L}^{\perp q}(x) H_1^{\perp q}(z). \tag{4}$$

The distribution function giving rise to SSA, $h_{1L}^{\perp}$, is related to the real part of the interference of wave functions for different orbital momentum states, and describes transversely polarized quarks in the longitudinally polarized nucleon. The physics of σ_{UL}, which involves the Collins fragmentation function $H_1^{\perp}$ and Ralston-Soper-Mulders-Tangerman (RSMT) distribution function $h_{1L}^{\perp}$, was first discussed by Kotzinian and Mulders in 1996 [2, 40, 38]. The same distribution function is accessible in double polarized Drell-Yan, where it gives rise to the $\cos 2\phi$ azimuthal moment in the cross section [42]. The behavior of the RSMT distribution function was recently studied in large-x [43] and large N_c [44] limits of QCD and large P_T of hadrons [45]. Positivity bounds on TMD distributions were also defined at leading order [46].

Measurements of the $\sin 2\phi$ SSA [38], allows the study of the Collins effect with no contamination from other mechanisms. A recent measurement of the $\sin 2\phi$ moment of σ_{UL} by HERMES [23] is consistent with zero. A measurably large asymmetry has been predicted only at large x ($x > 0.2$), a region well-covered by JLab [47].

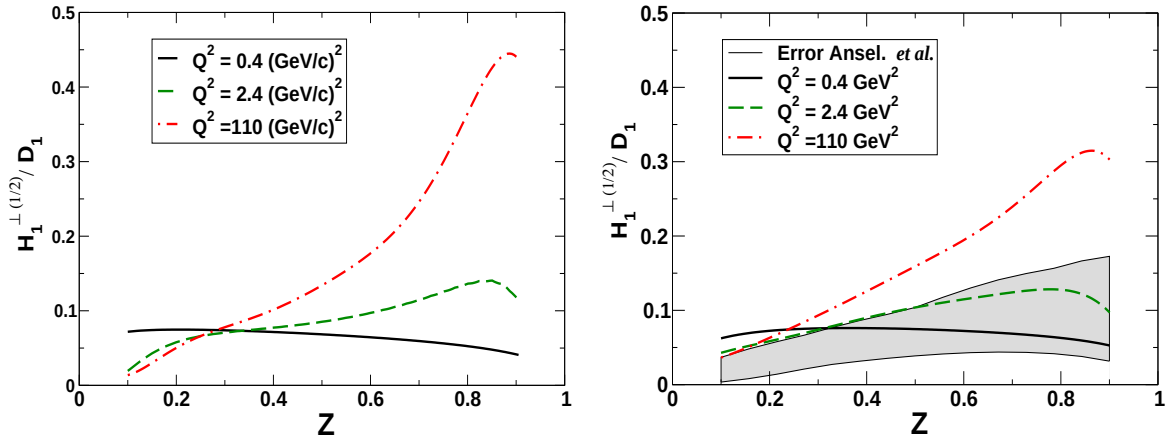

Figure 3: $H_1^{\perp(1/2)}/D_1$ for $u \to K^+$ (left) and π^+ (right) in the model of Bacchetta et al.[49], at the model scale (solid line) and at two other scales (dashed and dot-dashed lines) under the assumption that the Collins function does not evolve with the scale.

The extraction of the RSMT transverse momentum dependent distribution is complicated by the presence of an essentially unknown Collins function. Recently a significant asymmetry was measured by Belle [33] in e^+e^- annihilation to pions, indicating that the Collins function is indeed large.

Based on the leading order, a procedure has been developed recently [48] to extract the transversity distribution, combining e^+e^- and semi-inclusive DIS data [25]. The statistics, however, are not enough to make statistically significant predictions in the valence region, where the effects are expected to be large.

So far no experimental information is available about the Collins fragmentation function for kaons. Recent direct calculations of kaon Collins function [49] indicated that it may be comparable with pion Collins function (see Fig.3). HERMES measurements of the Collins asymmetry for pions and kaons, though, with large uncertainties, indicate that the differences may be significant.

Since pions and kaons are both Goldstone bosons of chiral symmetry breaking, In the chiral limit one has

$$\lim_{m_K \to 0} \frac{H_1^{\perp(1/2)a/K}}{D_1^{a/K}} = \lim_{m_\pi \to 0} \frac{H_1^{\perp(1/2)a/\pi}}{D_1^{a/\pi}} \,, \tag{5}$$

where $H_1^{\perp(1/2)}$ means integration over the transverse momentum weighted with k_T. Predictions for kaon Collins asymmetries assume the following relations to hold approximately

$$\frac{H_1^{\perp(1/2)\bar{s}/K^+}}{D_1^{\bar{s}/K^+}} \approx \frac{H_1^{\perp(1/2)u/K^+}}{D_1^{u/K^+}} \approx \frac{H_1^{\perp(1/2)u/\pi^+}}{D_1^{u/\pi^+}} \,,$$

$$\frac{H_1^{\perp(1/2)\mathrm{unf}/K^+}}{D_1^{\mathrm{unf}/K^+}} \approx \frac{H_1^{\perp(1/2)\mathrm{unf}/\pi^+}}{D_1^{\mathrm{unf}/\pi^+}} \,, \tag{6}$$

where it is understood that the fragmentation of d- and $\bar{u}$-flavour into K^+ is unfavoured.

Simultaneous measurements of the Kotzinian-Mulders asymmetry for pions and kaons will provide an independent measurement of ratios of Collins functions of pions and kaons, providing complementary measurements to e^+e^- annihilation.

The $\sin 2\phi$ moments ($\langle \sigma_{UL}^{\sin 2\phi} \rangle \equiv \sigma_{KM}$) in the polarized cross section, coming from the polarized fragmentation for different hadrons in the leading order for hydrogen (p) and neutron (n) targets are given by:

$$\sigma_{KM}^{\pi+}(p) = 4h_{1L}^{\perp u} H_1^{\perp(1/2)fav} + h_{1L}^{\perp d} H_1^{\perp(1/2)unfav} \tag{7}$$
$$\sigma_{KM}^{\pi-}(p) = 4h_{1L}^{\perp u} H_1^{\perp(1/2)unfav} + h_{1L}^{\perp d} H_1^{\perp(1/2)fav} \tag{8}$$
$$\sigma_{KM}^{\pi 0}(p) = 4(h_{1L}^{\perp u} + h_{1L}^{\perp d})(H_1^{\perp(1/2)unfav} + H_1^{\perp(1/2)fav}) \tag{9}$$
$$\sigma_{KM}^{K+}(p) = 4h_{1L}^{\perp u} H_1^{\perp(1/2)u/K^+} + h_{1L}^{\perp d} H_1^{\perp(1/2)d/K^+} + h_{1L}^{\perp \bar{s}} H_1^{\perp(1/2)\bar{s}/K^+} \tag{10}$$
$$\sigma_{KM}^{K-}(p) = 4h_{1L}^{\perp u} H_1^{\perp(1/2)u/K^-} + h_{1L}^{\perp d} H_1^{\perp(1/2)d/K^-} + h_{1L}^{\perp s} H_1^{\perp(1/2)s/K^-} + 4h_{1L}^{\perp \bar{u}} H_1^{\perp(1/2)\bar{u}/K^-} \tag{11}$$
$$\sigma_{KM}^{\pi+}(n) = 4h_{1L}^{\perp d} H_1^{\perp(1/2)fav} + h_{1L}^{\perp u} H_1^{\perp(1/2)unfav} \tag{12}$$
$$\sigma_{KM}^{\pi-}(n) = 4h_{1L}^{\perp d} H_1^{\perp(1/2)unfav} + h_{1L}^{\perp u} H_1^{\perp(1/2)fav} \tag{13}$$
$$\sigma_{KM}^{\pi 0}(n) = (4h_{1L}^{\perp d} + h_1^{\perp u})(h_{1L}^{\perp(1/2)unfav} + H_1^{\perp(1/2)fav}) \tag{14}$$
$$\sigma_{KM}^{K+}(n) = 4h_{1L}^{\perp d} H_1^{\perp(1/2)u/K^+} + h_{1L}^{\perp u} H_1^{\perp(1/2)d/K^+} + h_{1L}^{\perp \bar{s}} H_1^{\perp(1/2)\bar{s}/K^+} \tag{15}$$
$$\sigma_{KM}^{K-}(n) = 4h_{1L}^{\perp d} H_1^{\perp(1/2)u/K^-} + h_{1L}^{\perp u} H_1^{\perp(1/2)d/K^-} + h_{1L}^{\perp s} H_1^{\perp(1/2)s/K^-} + h_{1L}^{\perp \bar{u}} H_1^{\perp(1/2)\bar{u}/K^-} \tag{16}$$

Assuming that the transverse spin of the sea quarks in longitudinally polarized nucleon is negligible ($h_{1L}^{\perp \bar{q}} = 0$) and ignoring the non-valence quark contributions in K^+ production and unfavored fragmentation, the single-spin transverse asymmetry arising from fragmentation becomes:

$$A_{UL}^{K^+} \propto \frac{4h_{1L}^{\perp(1)u}(x)}{4u(x) + \bar{d}(x)} \frac{H_1^{\perp u \to K^+}(z, P_\perp)}{D_1^{u \to K^+}(z, P_\perp)}, \tag{17}$$

where $h_{1L}^{\perp(1)}$ means integration over the transverse momentum weighted with k_T^2. Similar formulas are available for neutron target replacing u and d, and also for K^-. For these, however, the contribution from unfavored fragmentation will be significant and should be accounted in the extraction.

Assuming isospin and charge-conjugation relations, there are in principle seven independent Collins fragmentation functions, but based on the observation that the pion favored Collins function is roughly equal and opposite to the unfavored one, the number of independent Collins functions could be reduced to three.

The asymmetries built from the difference between π^+ and π^- and of the K^+ and K^-

observables give (see Appendix-I)

$$A^{p/(\pi^+-\pi^-)}(x,y,z) = 2\frac{B(y)}{A(y)}\frac{\left(4\,h^{u_v}-h^{d_v}\right)H_1^{\perp(1)\mathrm{f}}}{\left(4\,f_1^{u_v}-f_1^{d_v}\right)\left(D_1^{\mathrm{f}}-D_1^{\mathrm{d}}\right)}, \tag{18}$$

$$A^{n/(\pi^+-\pi^-)}(x,y,z) = 2\frac{B(y)}{A(y)}\frac{\left(4\,h^{d_v}-h^{u_v}\right)H_1^{\perp(1)\mathrm{f}}}{\left(4\,f_1^{d_v}-f_1^{u_v}\right)\left(D_1^{\mathrm{f}}-D_1^{\mathrm{d}}\right)}, \tag{19}$$

$$A^{p/(K^+-K^-)}(x,y,z) = 2\frac{B(y)}{A(y)}\frac{4\,h^{u_v}\,H_1^{\perp(1)\mathrm{fd}}-h^{s_v}\,H_1^{\perp(1)\mathrm{f}'}}{4\,f_1^{u_v}\left(D_1^{\mathrm{fd}}-D_1^{\mathrm{dd}}\right)+f_1^{s_v}\left(D_1^{\mathrm{d}'}-D_1^{\mathrm{f}'}\right)}, \tag{20}$$

$$A^{n/(K^+-K^-)}(x,y,z) = 2\frac{B(y)}{A(y)}\frac{4\,h^{d_v}\,H_1^{\perp(1)\mathrm{fd}}-h^{s_v}\,H_1^{\perp(1)\mathrm{f}'}}{4\,f_1^{d_v}\left(D_1^{\mathrm{fd}}-D_1^{\mathrm{dd}}\right)+f_1^{s_v}\left(D_1^{\mathrm{d}'}-D_1^{\mathrm{f}'}\right)}. \tag{21}$$

The s_v superscript refers to the difference between s and $\bar{s}$. $A(y)$ and $B(y)$ are kinematic factors [3].

Neglecting the s_v contributions and the "unfavored " D_1^{dd} fragmentation function (FF), the "kaon differences" asymmetries simplify to

$$A^{p/(K^+-K^-)}(x,y,z) = 2\frac{B(y)}{A(y)}\,\frac{h^{u_v}}{f_1^{u_v}}\,\frac{H_1^{\perp(1)\mathrm{fd}}}{D_1^{\mathrm{fd}}}, \tag{22}$$

$$A^{n/(K^+-K^-)}(x,y,z) = 2\frac{B(y)}{A(y)}\,\frac{h^{d_v}}{f_1^{d_v}}\,\frac{H_1^{\perp(1)\mathrm{fd}}}{D_1^{\mathrm{fd}}}. \tag{23}$$

where the index "fd" indicates favored kaon FFs. The z dependence of the above asymmetries is predicted to follow the curve in Figure 3.

In the approximation of strangeness contribution being negligible in the valence region one can write:

$$\frac{H_1^{u/K+}-H_1^{u/K-}}{H_1^{u/\pi+}-H_1^{u/\pi-}} = \frac{15}{4}\frac{F_p^{K+}-F_p^{K-}}{3(F_p^{\pi+}-F_p^{\pi-})+(F_d^{\pi+}-F_d^{\pi-})}, \tag{24}$$

where F_{target}^{hadron} can be any one of four Collins asymmetries related to $H_1^{\perp}$, like $\langle\cos 2\phi\rangle_{UU}$, $\langle\sin 2\phi\rangle_{UL}$, $\langle\sin(\phi+\phi_S)\rangle_{UT}$ or $\langle\sin(3\phi-\phi_S)\rangle_{UT}$.

There are indications from Collins asymmetry measurements [25] that $H_1^{u/\pi+}-H_1^{u/\pi-}$ is large, and that will allow precision measurement of kaon Collins function, under the assumptions discussed above. That measurement will also provide a check of chiral limit prediction, where that ratio is expected to be at unity. More ratios could be constructed from other observable moments with pions and kaons on proton and deuteron targets. With a given Collins function, one can study all involved TMD distributions.

Measurements of transverse momenta of final state hadrons in SIDIS with longitudinally polarized targets will thus provide information on the polarized Collins fragmentation of kaons complementary to transverse target and future measurements in e^+e^- by BELLE.

Measurements of transverse momentum dependence of helicity distributions will be also important for interpretation of ongoing studies at different facilities worldwide of gluon polarization using high P_T hadrons [50, 51, 52, 53].

We propose a measurement of azimuthal moments of the single kaon cross section in SIDIS using the CLAS12 detector in Hall B at Jefferson Lab, a 6.6-11.0 GeV longitudinally polarized electron beam and longitudinally polarized hydrogen and deuterium targets. The main focus of this proposal is to study the $\sin 2\phi$ asymmetry, related to the correlation of intrinsic transverse momentum of quarks and their transverse spin.

The overall statistics of kaons is almost an order of magnitude less than for pions with most of the relevant sources of systematic errors being the same, so the main focus will be the new information we can access with kaon SIDIS measurements and in particular studies of the Collins fragmentation of kaons. We propose to run with high luminosity, $\sim 10^{35}$ $\mathrm{cm}^{-2}\mathrm{s}^{-1}$, yielding an integrated luminosity of ~ 500 fb^{-1}.

1.1.2 Subleading-twist azimuthal and spin asymmetries

So far only leading twist observables were discussed. However, it is worth to recall that

- the first evidence for azimuthal asymmetries in unpolarized SIDIS was the azimuthal asymmetry $A_{UU}^{\cos\phi}$ observed at EMC [54],
- the first evidence for SSAs in SIDIS was the longitudinal target SSA $A_{UL}^{\sin\phi}$ observed at HERMES initially $\pi^{\pm}$ produced from proton [23, 55] later also $\pi^{\pm}$, π^0, $K^{\pm}$ from proton and deuteron targets [24, 56], see also [57],
- the first SSA in SIDIS of a longitudinally polarized electron beam off a unpolarized target was the asymmetry $A_{LU}^{\sin\phi}$ observed at CLAS [28] confirmed later by HERMES [26].
- the first preliminary results on double-spin azimuthal asymmetries in SIDIS of a longitudinally polarized electron beam off a longitudinally polarized target ($A_{LL}^{\cos\phi}$) have been reported by CLAS [58].

What these observables have in common is that, if one assumes factorization, they are given in a tree-level formalism in terms of twist-3 TMDs. Corresponding structure functions are listed in the Appendix-II.

Measurements of these observables are of interest for several reasons.

The partonic description of these structure functions was initiated in [2] and completed more recently [59, 60, 61, 62, 63, 64], after it was recognized that a most general description of the light-front correlators which defines TMDs contains additional Lorentz-structures due to the gauge-link [65]. Presently it is not known whether factorization proven for leading-twist observables in SIDIS holds also at subleading twist [66]. Assuming that, the sub-leading observables (60-63) provide unique insights into the quark-gluon-quark dynamics, which is of interest by itself [67].

The asymmetry $A_{UL}^{\sin\phi}$ played an important role for the early understanding of SSAs in SIDIS [68, 69, 70, 71, 72, 73, 74, 75], when it was believed that it is mainly due to the Collins effect (incorrectly at those times — especially due underestimating the role of the unfavoured Collins fragmentation function). A revised description of this observable contains additional structures [59, 60, 61, 62, 63, 64, 65]. A first step towards an understanding of this SSA

could therefore consist in choosing another approximation, namely the neglect of quark-gluon-quark terms which are pure twist-3 ('tilde-functions') or current quark mass terms. Such an approximation works well in the case of the twist-3 distribution function $g_T(x)$ [76]. In the case of $g_T(x)$ this approximation is referred to as Wandzura-Wilczek approximation [77]. If one applies this approximation to $A_{UL}^{\sin\phi}$ the only term which is left is due to h_L and $H_1^\perp$ with $h_L(x) \approx 2x \int_x^1 dy \frac{h_1(y)}{y^2}$ [78, 79]. The latter approximation, which allows to express $h_L(x)$ in terms of $h_1(x)$ is motivated by studies in the instanton model of the vacuum [80]. However, the contribution of h_L and $H_1^\perp$ to the SSA accounts for only a small fraction of the observed effect [81]. New data on $A_{UL}^{\sin\phi}$ would give valuable insights on the mechanisms behind this SSA.

The SSA $A_{LU}^{\sin\phi}$ is equally interesting. Before it became clear that the are additional structures [59, 60, 61, 62, 63, 64, 65] the SSA was believed to be due to the twist-3 function $e(x)$ and the Collins function [2], and 'first indications' on it were extracted [47] from the CLAS data [28]. What makes $e(x)$ interesting is that its first moment is connected to the pion-nucleon sigma-term [78] and arises solely due to a δ-function-type singularity at $x = 0$ [82]. In practice this singularity would manifest itself as a mismatch of the theoretical expectation for the value of this moment, and the result measured for $x > 0$ [82]. Moreover, $e(x)$ has also been related to the transverse force experienced by a transversely polarized quark ejected from a transversely polarized nucleon [67]. Of course, in the complete description of this observable additional structures enter. Interestingly all structures in this SSA are, explicitly or implicitly, due to quark-gluon-quark terms or current quark mass terms. If such terms were really small, as advocated sometimes in literature [83, 84], this SSA would be zero — in contrast to what data show [28, 26]. Significant effect has been predicted also for azimuthal modulations of the double-spin asymmetry DSA $A_{LL}^{\cos\phi}$ in a Cahn-effect-approximation [37].

As a by-product, the proposed experiment will provide data on sub-leading asymmetries which would provide valuable insights, and especially provide an answer to the interesting question why subleading twist effects appear to be larger then leading twist effects ($A_{UU}^{\cos\phi}$ was larger than $A_{UU}^{\cos 2\phi}$ [54], $A_{UL}^{\sin\phi}$ was larger than $A_{UL}^{\sin 2\phi}$ [23]). Precise data on the production of pions and kaons would have an important impact, and motivate further theoretical studies.

1.2 Transverse momentum dependence of partonic distributions

Assuming the Gaussian ansatz for distribution and fragmentation functions ($D_1(z, \mathbf{K}_T) = D_1^a(z)\, \exp(-\mathbf{K}_T^2/\langle K_{D_1}^2\rangle)/\pi\langle K_{D_1}^2\rangle$ and $f_1^a(x, \mathbf{p}_T) = f_1^a(x)\, \exp(-\mathbf{p}_T^2/\langle \mathbf{p}_T^2\rangle)/\pi\langle \mathbf{p}_T^2\rangle$) in the approximation of flavor and x or z-independent widths, a good quantitative description of data was obtained [85] for

$$\langle p_T^2\rangle = 0.25\,\mathrm{GeV}^2\,, \quad \langle K_{D_1}^2\rangle = 0.20\,\mathrm{GeV}^2\,. \tag{25}$$

Assuming the Gaussian model the average $P_{h\perp}$ of hadrons produced in SIDIS is given by

$$\langle P_{h\perp}(z)\rangle \;=\; \frac{\sqrt{\pi}}{2}\,\sqrt{z^2\langle p_T^2\rangle + \langle K_{D_1}^2\rangle}\,. \tag{26}$$

A satisfactory description with HERMES data [56] on deuteron was obtained [86] with

$$\langle p_T^2\rangle = 0.33\,\mathrm{GeV}^2\,, \quad \langle K_{D_1}^2\rangle = 0.16\,\mathrm{GeV}^2\,. \tag{27}$$

TMD	$\langle p_T \rangle$ in GeV	$\langle p_T^2 \rangle$ in GeV^2	$\frac{4\langle p_T \rangle^2}{\pi \langle p_T^2 \rangle}$
f_1	0.239	0.080	0.909
g_1	0.206	0.059	0.916
h_1	0.210	0.063	0.891
$g_{1T}^{\perp}$	0.373	0.176	1.007
$h_{1L}^{\perp}$	0.373	0.176	1.007
$h_{1T}^{\perp}$	0.190	0.050	0.919

Table 2: The mean transverse momenta and the mean square transverse momenta of T-even TMDs, from the constituent quark model [88]. If the transverse momenta in the TMDs were Gaussian, then the result for the ratio in the last row would be unity, see text.

TMD	$\frac{\langle p_T^2 \rangle}{\langle p_{Tf_1}^2 \rangle}$
f_1	1.00
g_1	0.74
h_1	0.79
$g_{1T}^{\perp}$	2.20
$h_{1L}^{\perp}$	2.20
$h_{1T}^{\perp}$	0.63

Table 3: Mean square transverse momenta of T-even TMDs, from the constituent quark model [88] in units of the mean square transverse momenta of f_1, denoted as $\langle p_{Tf_1}^2 \rangle$. These numbers are considered to be a more robust model prediction.

The width for different partonic distributions can be different. Values for different T-even partonic distributions, computed [87] in the constituent quark model [88] are listed in Table 2. Values normalized to the width of the unpolarized distribution function are listed in Table 3.

Future measurements of azimuthal moment as a function of P_T in different bins in x, z, Q^2 combined with measurements of azimuthal moments of the unpolarized cross section proposed for `CLAS12` in case of pions [89, 39], will allow for study of the flavor dependence of transverse momentum distributions. These measurements will provide access to widths in transverse momentum of different underlying partonic distributions. Measurements with kaons will provide important independent information on width of different partonic distributions giving rise to corresponding azimuthal moments.

In order to perform a P_T-dependent flavor decomposition double spin asymmetries have to be extracted in bins in P_T. The P_T-dependent cross section is given by[37]:

$$\sigma_{LL} = \frac{\pi}{xy^2}\left[\, y(2-y)\,\right] \Sigma_q e_q^2 \int d^2\mathbf{p}_\perp\; g_{1L}^q(x,\mathbf{p}_\perp)\; D_q^h(z,\mathbf{P}_{hT}-z\mathbf{p}_\perp)\;, \tag{28}$$

$$\sigma_0 = \frac{\pi}{xy^2}\left[\, 1+(1-y)^2\,\right] \Sigma_q e_q^2 \int d^2\mathbf{p}_\perp\; f_1^q(x,\mathbf{p}_\perp)\; D_q^h(z,\mathbf{P}_{hT}-z\mathbf{p}_\perp)\;. \tag{29}$$

Assuming a Gauss model for the polarized structure function and $A_{LL} = F_{LL}/F_{UU}$ one can write [87]:

$$F_{LL}(x,z,P_{h\perp}) = \sum_a e_a^2\, x g_1^a(x)\, D_1^a(z)\; \frac{\exp(-P_{h\perp}^2/\langle P_{h\perp}^{2,\mathrm{pol}}\rangle)\rangle}{\pi\;\langle P_{h\perp}^{2,\mathrm{pol}}\rangle} \tag{30}$$

with

$$\langle P_{h\perp}^{2,\mathrm{pol}}\rangle = \langle K_T^2\rangle + z^2\langle p_T^2(g_1)\rangle\;, \tag{31}$$

where $\langle p_T^2(g_1)\rangle$ denotes the Gaussian width of the helicity distribution function.

Assuming that the widths are flavour and x or z-independent, then the double spin asymmetry is given by

$$A_{LL}(x,z,P_{h\perp}) = A_{LL}(x,z)\; \frac{\langle P_{h\perp}^{2,\mathrm{unp}}\rangle}{\langle P_{h\perp}^{2,\mathrm{pol}}\rangle}\; \exp\!\left(P_{h\perp}^2/\langle P_{h\perp}^{2,\mathrm{unp}}\rangle - P_{h\perp}^2/\langle P_{h\perp}^{2,\mathrm{pol}}\rangle\right), \tag{32}$$

and we define the 'multiplicities asymmetry'

$$a_{LL}(P_{h\perp}) = \frac{\langle\langle F_{LL}(x,z,P_{h\perp})\rangle\rangle}{\langle\langle F_{LL}(x,z)\rangle\rangle} = \frac{\langle P_{h\perp}^{2,\mathrm{unp}}\rangle}{\langle P_{h\perp}^{2,\mathrm{pol}}\rangle}\; \exp\!\left(P_{h\perp}^2/\langle P_{h\perp}^{2,\mathrm{unp}}\rangle - P_{h\perp}^2/\langle P_{h\perp}^{2,\mathrm{pol}}\rangle\right). \tag{33}$$

Similar for the polarized 'multiplicities':

$$\langle n(P_{h\perp})\rangle_{LL} = \frac{1}{F_{LL}}\,\frac{\mathrm{d}F_{LL}}{\mathrm{d}P_{h\perp}} = \frac{\langle\langle 2\pi P_{h\perp}\, F_{LL}(x,z,P_{h\perp})\rangle\rangle}{\langle\langle F_{LL}(x,z)\rangle\rangle} = 2\,P_{h\perp}\,\frac{\exp(-P_{h\perp}^2/\langle P_{h\perp}^{2,\mathrm{pol}}\rangle)}{\langle P_{h\perp}^{2,\mathrm{pol}}\rangle} \tag{34}$$

normalized as $\int \mathrm{d}P_{h\perp}\langle n(P_{h\perp})\rangle_{LL} = 1$. Then the 'multiplicities asymmetry' would be given by:

$$a_{LL}(P_{h\perp}) = \frac{\langle n(P_{h\perp})\rangle_{LL}}{\langle n(P_{h\perp})\rangle_{UU}}\;. \tag{35}$$

The a_{LL}, assuming the ratio $\langle p_{T,g_1}^2\rangle/\langle p_{T,f_1}^2\rangle = 0.74$ (Table 3), is shown in Fig. 4b. Predictions show little dependence on the choice of parameters, Eq. (25) vs. (27). The prediction in Fig. 4b depends more strongly on the model prediction. The prediction is independent of the target and produced hadron. Measurements with Kaons on hydrogen and deuteron targets, thus can provide an independent measurement of widths.

Precise measurements of the observables $\langle n(P_{h\perp})\rangle$ and a_{LL} will provide us with important insights on the dynamics in the transverse plane.

Measured single and double spin asymmetries for all pions and kaons in a large range of kinematic variables (x_B, Q^2, z, $P_\perp$, and ϕ), combined with measurements with unpolarized targets, will provide detailed information on the flavor and polarization dependence of the

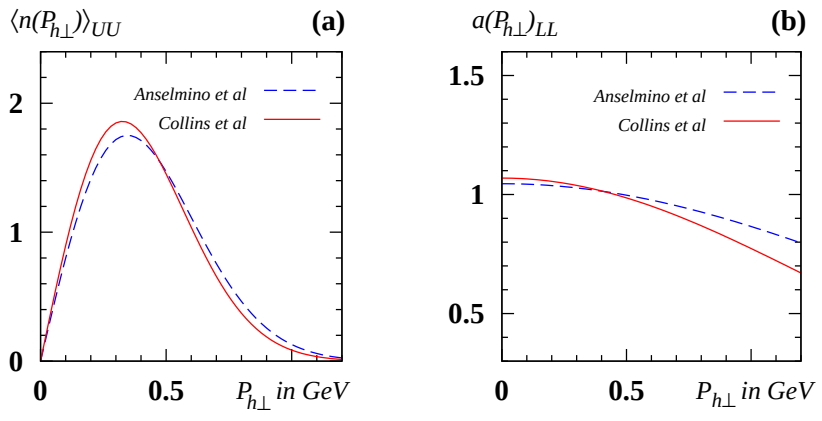

Figure 4: (a) The transverse hadron momentum dependent multiplicities $\langle n(P_{h\perp})\rangle_{UU}$ calculated on the basis of the phenomenological results in Eqs. (25, 27) [87], (b) Normalized P_T-dependence due to difference in f_1 and g_1 widths.

transverse momentum distributions of quarks in the valence region, and in particular, on the x_B, z, and $P_\perp$ dependence of the leading TMD parton distribution functions of u and d quarks. Such measurements across a wide range of x, Q^2, and P_T would allow for detailed tests of QCD dynamics in the valence region complementing the information obtained from inclusive DIS. They would also serve as novel tools for exploring nuclear structure in terms of the quark and gluon degrees of freedom of QCD.

1.3 Data on azimuthal moments and helicity structure

Measurements of longitudinal spin dependent moments are available from HERMES and JLab. The preliminary data from CLAS at 6 GeV indeed indicate large azimuthal moments both for $\sin\phi$ and $\sin 2\phi$. The data on kinematic dependence of the leading-twist SSA are shown in Fig. 5. Calculations were done using $h_{1L}^\perp$ from the chiral quark soliton model evolved to Q^2=1.5 GeV^2 [47], f_1 from GRV95 [90], and D_1 from Kretzer, Leader, and Christova [91]. The Collins function obtained from fit [92] to HERMES and Belle data was used to calculate the curves, and the band correspond to the uncertainty on the Collins function. An important ingredient for the estimates are the so-called "Lorentz-invariance relations" that connect $h_{1L}^\perp$ with h_1 [2]. Although these relations are known not to be valid exactly [65, 64]. It is of importance to find out experimentally to which extent such relations can provide useful approximations, or whether they are badly violated, since there is little theoretical intuition on that point.

The kinematic dependence of the SSA for π^+, measured from the CLAS EG1 data set at 6 GeV is consistent with predictions [47]. The π^+ SSA is dominated by the u-quarks. Therefore with some assumption about the ratio of unfavored to favored Collins fragmentation functions, it can provide a first glimpse of the RSMT TMD function. The distribution function $h_{1L}^\perp$ was extracted using the π^+ target SSA [29], which is less sensitive to the unknown ratio of unfavored (d-quark fragmenting to π^+) to favored (u-quark fragmenting to

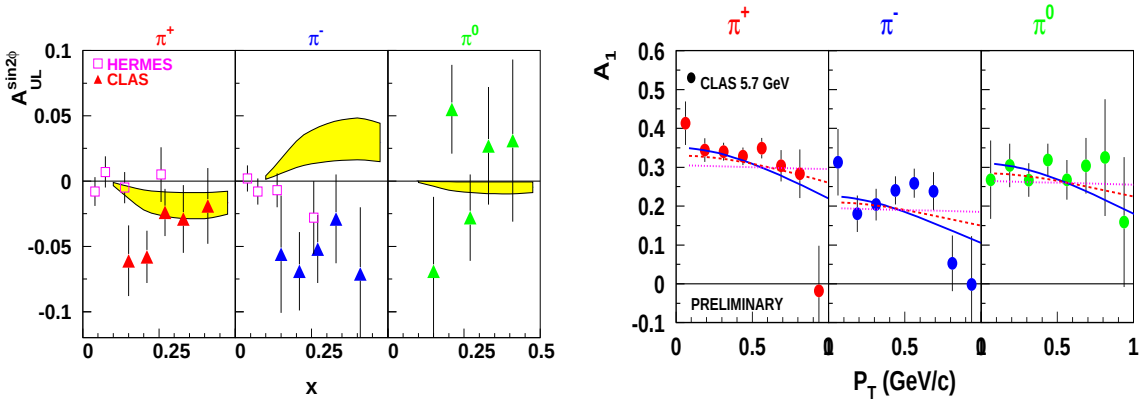

(a) (b)

Figure 5: Measurements of single (left) and double (right) spin asymmetries as a function of x and P_T. The open squares show the HERMES data, and filled symbols are for CLAS preliminary results at 5.7 GeV. The curves are calculated using Ref. [96](a) and [37] (b).

π^+) polarized fragmentation functions. The extraction requires knowledge of the ratio of the Collins favored and unfavored fragmentation functions. Combination of hydrogen and deuterium measurements will provide a set of equation (similar to Eq.16) allowing extraction of ratios of different flavor components of both distribution (ex. h_{1L}^d/h_{1L}^u), and fragmentation functions. Measurements with kaons will provide additional information on kaon Collins functions.

Measurements of transverse momenta of final state hadrons in SIDIS with longitudinally polarized targets will provide complementary to transverse target information, probing the longitudinal nucleon structure beyond the collinear approximation. The $P_\perp$-dependence of the double-spin asymmetry, measured for different bins in z and x will provide a test of the factorization hypothesis and probe the transition from the non-perturbative to perturbative description. At large P_T ($\Lambda_{QCD} << P_T << Q$) the asymmetry is expected to be independent of $P_\perp$ [12].

There are indications that the double-spin asymmetry (see Fig. 5) at small P_T tends to increase for π^- and decrease for π^+. A possible interpretation of the P_T-dependence of the double spin asymmetry may involve different widths of transverse momentum distributions of quarks with different flavor and polarization [37] resulting from a different orbital structure of quarks polarized in the direction of the proton spin and opposite to it [93, 94]. This interpretation may demand a different width for d-quarks than for u-quarks, consistent with observation from lattice QCD studies of a different spread in transverse distances for d-quarks compared to u-quarks [95]. The same effect may be responsible for the relatively large $\cos\phi$ moment of the double spin asymmetry.

Preliminary data on P_T-dependence for all hadrons and hydrogen and deuterium targets is available from HERMES, however the statistics in the valence region, where the effects

are expected to be significant, doesn't allow for drawing definitive conclusions.

Detailed measurements of A_{LL} and its $\cos\phi$ moment as a function of P_T in different bins [39] in x, z, Q^2 combined with measurements of azimuthal moments of the unpolarized cross section proposed for `CLAS12` will allow study of the flavor dependence of transverse momentum distributions.

The goal of our proposed experiment is to gather a data set on kaon SIDIS in the region $0.1 \leq x \leq 0.8$, $0 \leq P_T \leq 1.2$, and $0.2 \leq z \leq 0.8$. Global analysis of the data will provide fits to transverse momentum dependent helicity distributions. The CLAS12 RICH upgrade will allow detection of kaons over the full kinematic range, allowing studies of the effect of strange and non-strange sea on the flavor and spin structure of the nucleon.

2 Experimental details

2.1 CLAS12

The proposed experiment will use the upgraded CLAS12 spectrometer with two sectors of the low threshold Cherenkov counter replaced by proximity RICH detectors. We will run at the standard magnetic field. Running conditions will be similar to an already approved CLAS12 proposal for semi-inclusive DIS studies with CLAS12 [97, 39] for longitudinally polarized proton and deuteron targets. The central tracker will also be used for coincident detection of protons and pions. The solenoid for the central tracker is also used simultaneously to provide the magnetic field for the polarized target. Additional details on CLAS12 can be found in the document provided as an appendix to all CLAS12 proposals.

2.2 CLAS12 Particle Identification

In the baseline design of CLAS12, particle identification in the forward detector is obtained by using the high threshold Cerenkov counter (HTCC), the low threshold Cerenkov counter (LTCC) and the Time-of-flight scintillator arrays (TOF). In the $2.5-5$ GeV/c momentum region, the π/K separation relies only on the LTCC performance. Moreover, in the $4-8$ GeV/c momentum region it is not possible to separate protons from kaons. Considering that at 12 GeV for semi-inclusive processes, the K/π ratio is of the order of $10-15\%$ and assuming a pion detection inefficiency for the LTCC of 10%, then the π/K rejection factor is $1:1$. In general, this PID system is well matched to requirements of the main physics program at 12 GeV. However there are some physics reactions of high interest, such as the one covered by this proposal, that cannot be easily accessed without better PID, especially for charged kaon detection. A RICH detector, to be installed in place of the low threshold Cerenkov counter, will significantly improve the CLAS12 particle identification overcoming the above limitations.

2.2.1 CLAS12 RICH detector

A proximity focusing RICH similar to the one operating in Hall A at Jefferson Lab [98, 99] and successfully working during the hyper-nuclear spectroscopy experiment [100], may represent an adequate choice to fulfill our requirements. Presently, we didn't take into account other possibilities, such as an aerogel RICH, due to the higher costs and additional technical constraints. A proximity focusing RICH detector will allow us a good separation of $\pi/K/p$ in the $2.5-5$ GeV/c momentum region, as demonstrated later on and, in addition, replacing part or full LTCC will not have any impact on the baseline design of CLAS12. Moreover, replacing LTCC with RICH has an advantage that it can be done module by module without interfering with detector construction of CLAS12 operations. In Fig. 6 a schematic layout of the proximity focusing RICH is reported. In the RICH operating in Hall A the photons are produced by over threshold particles in the liquid freon C_6F_{14} with a refractive index of 1.28 and thickness of 15 mm. Then they refract on a quartz window of 5 mm and diverge in a 160 mm proximity gap, filled by CH_4. Eventually they are converted to electrons by a thin layer of CsI (300 nm) deposited on five pad planes that represent the cathode of a

Multi-wire Proportional Chamber. The induced charge of the electric avalanche is readout on each pad by a sample and hold analogically multiplexed front-end electronics. Spatial information is obtained from the segmented pads, whose size is $8 \times 8.4\ mm^2$. One of the most

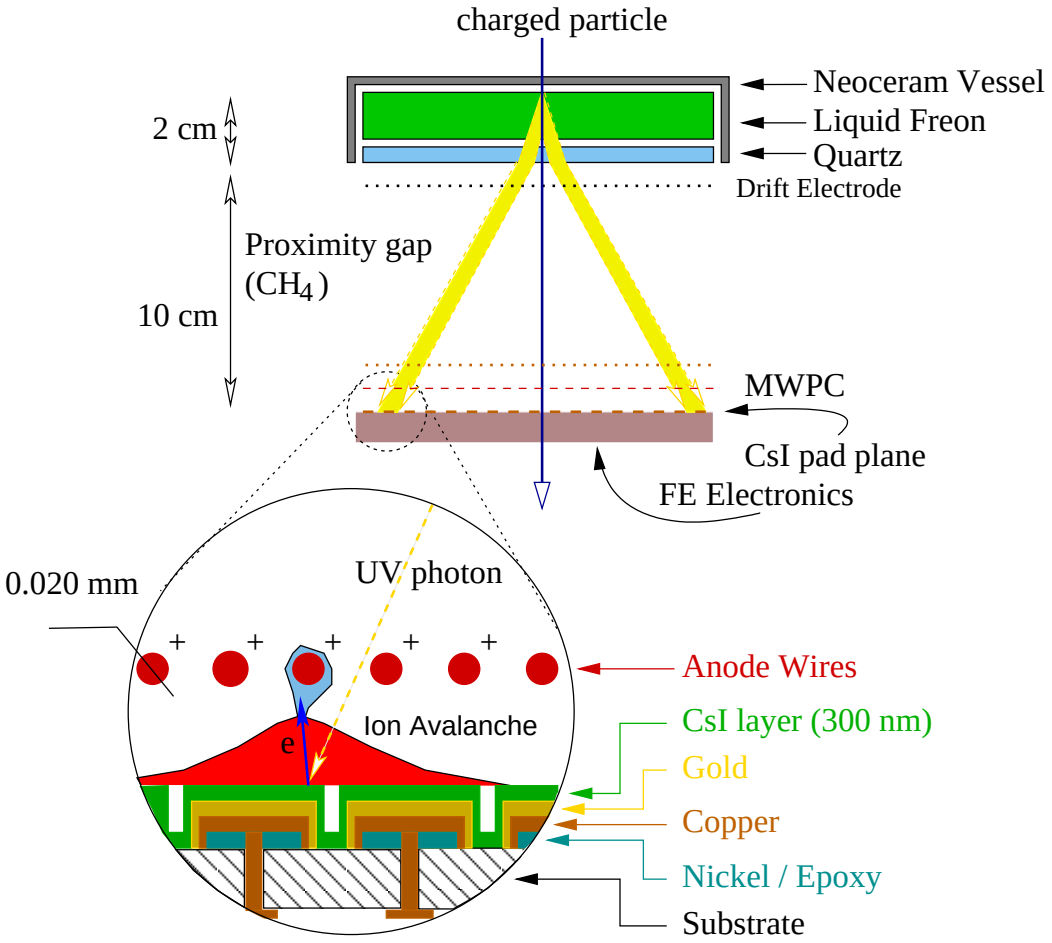

Figure 6: Schematic layout and working principle of the freon CsI proximity focusing RICH.

important aspect of the proximity focusing fluorocarbon/CsI RICH detector is represented by the deposition of a layer of photo-converted material (CsI) on the pad plane. This is obtained by means of the evaporation of a pure CsI powder or crystals in a high vacuum chamber. The INFN Rome group has built, installed and operated at JLab an evaporation chamber for large area pad (up to about 650 x 650 mm^2). A quantum efficiency (QE) online measurement system has also been integrated into the evaporation chamber. A typical measured QE is of the order of $20 - 25$ %.

Preliminary Monte Carlo studies based on GEANT3 [101] has been performed in order to optimize all the components of the detector: radiator thickness, gap length, radiator type. The main output parameter will be the mean error on Cerenkov angle reconstruction of kaons and pions; $\sigma_{K-\pi}$.

Assuming particles uniformly distributed in the phase space, results obtained for kaon-proton and kaon-pion separation versus the particle momentum are shown in Fig 7 for two

different radiators, C_5F_{12} and C_6F_{14}, respectively. In the plots the points refer to the Monte Carlo simulation while the curves are analytical functions. As we can see for the C_6F_{14} the $\sigma_{K-\pi}$ and σ_{K-p} are ~ 1 mrad larger than for the C_5F_{12} thus the use of the latter is mandatory. The disadvantage in using the freon C_5F_{12} is its need for cooling because it evaporates at 29° Celsius at standard temperature and pressure. In the simulation, the dimensions of the

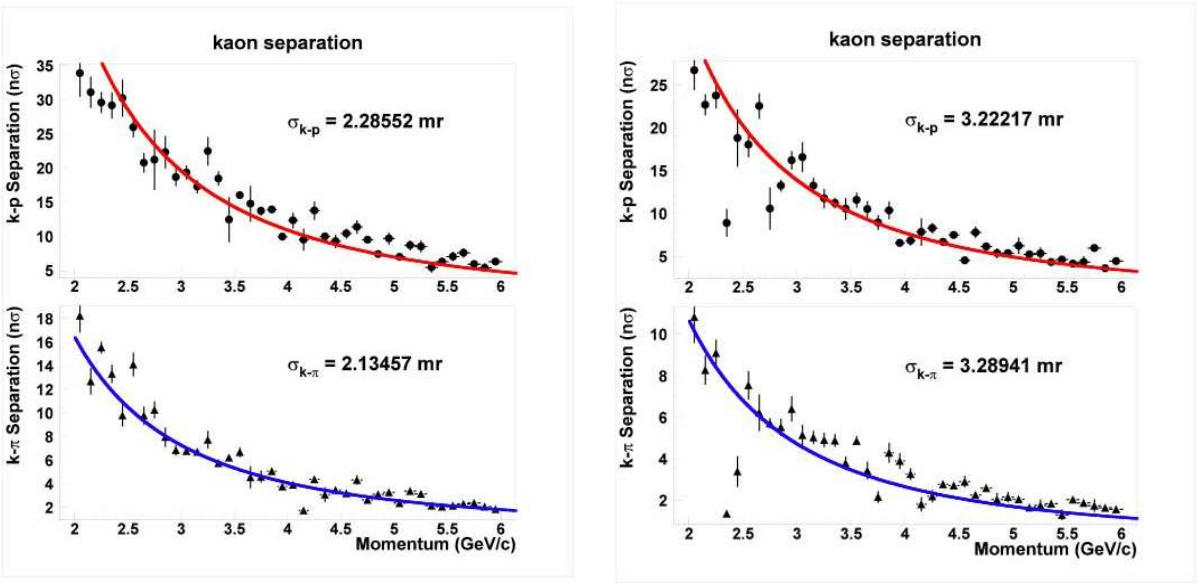

Figure 7: Left: Kaon-proton separation (upper plot) and kaon-pion separation (lower plot) versus the particle momentum for C_5F_{12}. The points refer to the Monte Carlo simulation while the curves are analytical functions. Right: Kaon-proton separation (upper plot) and kaon-pion separation (lower plot) versus the particle momentum for C_6F_{14}. The points refer to the Monte Carlo simulation while the curves are analytical functions.

radiator thickness and the gap length as well as the pad/pixel size of the photon detector have been varied in order to find the optimal combination which gives the smaller reconstruction error in the Cerenkov angle. It has been found that a freon thickness of ~ 3 cm, a gap length of ~ 80 cm and a pad size less than 1 cm minimize the $\sigma_{K-\pi}$ value. Finally, to determine the best photon detector size, pions, kaons and protons have been generated at the LTCC-RICH entrance window according to realistic phase space distributions. The positions at the detector level of all photons generated in the radiator has been studied for a radiator polar angle acceptance of $5° - 30°$. In Fig. 8 left, the black dots are the charged particle positions at the RICH entrance (the envelope is the radiator). The contour lines are the positions at the detector level of all photons generated in the radiator (different colors refer to different intensity) while the large arc is the detector surface (photons outside of there are not detected). Our final results for the mean error on the kaon Cerenkov angle reconstruction are shown in Fig. 8 (Right). We can achieve a 4σ $K-\pi$ separation at 5 GeV/c. Therefore, we will have 80% kaon detection efficiency with 1:1000 rejection factor (or 95% with 1:100 rejection factor). This study was performed for a single sector of CLAS12, with a radiator size $\leq 4m^2$ and a detector size of $\sim 14m^2$. For six sectors, the radiator size will be $\leq 24m^2$ while the detector size of $\sim 40m^2$. The total radiation thickness of the proposed RICH is

Table 4: Radiation lengths corresponding to the different parts of the RICH detector.

	Thickness (cm)	$X_0\%$
Entrance window		
Al	0.05	0.5
Rohacell51	5	2
Al	0.05	0.5
Radiator		
Neoceram	0.4	3
C_6F_{14}	3	15
Quartz	0.5	4
Gap		
CH_4	80	0.001
Photon Detector		
Pad NEMAG10	0.08	0.4
or		
GEM chamber	1	0.6

of the order of 30% X_0. In Table 4, the radiation lengths corresponding to different parts of the RICH detector are reported. A very preliminary cost estimate has been evaluated, based on the cost of the Hall A RICH detector. Taking into consideration the replacement of two adjacent LTCC sectors, it is found to be of the order of 2.5 M$. The crucial part to be funded is the liquid radiator C_5F_{12} for which a 0.8 M$ cost has been estimate (for the total quantity needed we have considered 5 times the volume of two sectors which is $\sim$ 250 l). Detailed information about the proposed RICH, its cost and parameters can be found in Ref. [102].

2.2.2 Kaon Identification with CLAS12 with TOF, LTCC and HTCC

A simulation was performed to study kinematic dependences of kaons detected using the Time-of-flight scintillator arrays (TOF) at low momenta ($P < 2.5$ GeV) and the high threshold Cerenkov counter at high kaon momenta ($P > 5$ GeV), assuming very high efficiency of the HTCC for pion detection. The relevant kinematic variables for semi-inclusive DIS are the x, y, z and the hadron transverse momentum with respect to the virtual photon P_T. While detection (identification) of kaons even in limited momentum range ($P < 2.5$ GeV and $P > 5$ GeV) will still allow a full coverage over the most accessible kinematics (see Fig.9) the statistics will be significantly less and distributions will be distorted. This is better seen for the the z and P_T-dependences of kaons, which are the most sensitive variables to the kaon momentum. The sectors of CLAS12 with no RICH will still provide a valuable for kaon studies data, but data from sectors covered by RICH will be very important to use them efficiently.

2.2.3 Advantages of the RICH

The best solution to improve K^+ and K^- identification and increase the statistics ($\sim$ a factor of 3) will be complimenting the PID system of forward detector with a Ring Imaging

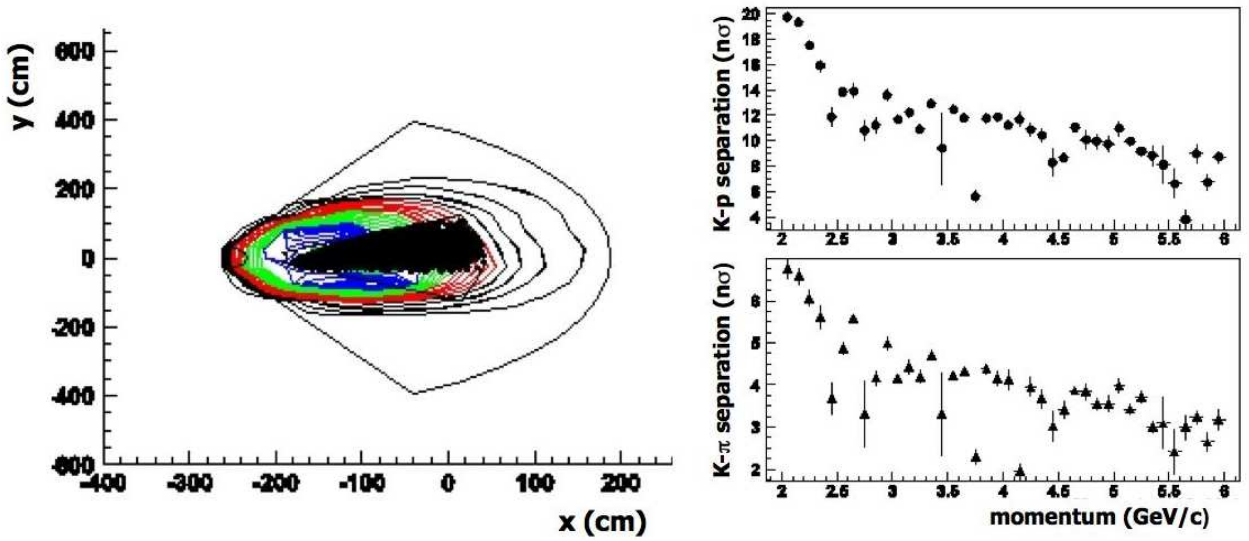

Figure 8: Left: Contour lines: positions at the detector level of all photons generated in the radiator for a polar angle acceptance of $5° - 30°$. The black dots are the charged particle positions at RICH entrance; the large arc is the detector surface. x/y are not to scale. Right: Kaon-proton separation (upper plot) and kaon-pion separation (lower plot) versus the particle momentum for C_5F_{12} and a radiator polar angle acceptance of $5° - 30°$.

Cerenkov counter.

The time of flight can separate between kaons and protons for momenta up to 4 GeV/c. The kaon to proton ratio obtained from PEPSI Monte-Carlo is shown in Fig. 10 in the region where time of flight is not helpful. The number of proton is at least twice the number of kaons making the argument for a RICH detector even stronger.

In addition to much needed PID for kaons at momenta $P > 2.5$ GeV, RICH will help to reduce accidental in high luminosity runs, when particles from different beam buckets can mix. In Fig. 11 leakage of protons (left graph) and pions (right graph) from different beam buckets into kaons is illustrated. At high luminosities, protons and pions that get produced at high rates will leak into kaon sample and measuring on TOF will not be enough to separate them.

2.2.4 The polarized target

The target configuration will be the same as for already approved proposals using the polarized target [97, 39]. It will be polarized via the method of Dynamic Nuclear Polarization (DNP) which is a well established technique that has been used extensively in nuclear and particle physics experiments, including the ones performed in Hall B of Jefferson Lab. Dynamically polarized target systems consist of a hydrogenated (polarized protons) or deuterated (polarized neutrons) compound containing paramagnetic centers, such as unpaired electrons, placed in a high magnetic field and cooled to low temperatures, with a B/T ratio of the order of 5 Tesla/Kelvin. In these conditions, the free electron spins can approach polarization of 100%. The high polarization of unpaired electrons is then transferred dynamically to the nucleons by irradiating the target material at frequency near that of electron spin resonance.

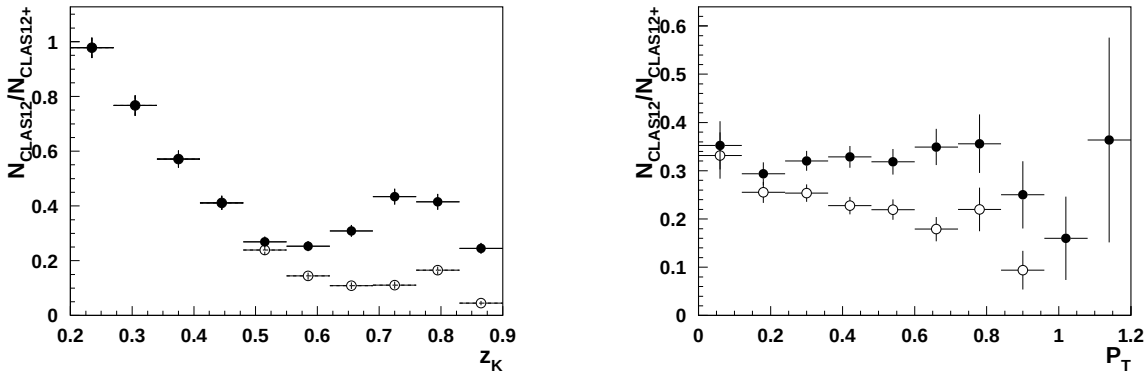

Figure 9: Relative gain of kaons with CLAS12 (with RICH) compared to the base CLAS12. The open circles assume only Kaons detected by TOF ($P < 2.5$ GeV), filled circles include both TOF and HTCC ($P > 5$ GeV). The left plot shows the z dependence while the right one shows the P_T distribution.

This technique typically achieves a proton polarization of 80-90%, and a deuteron polarization of 30-40%. The nucleons in the target will be polarized either parallel or anti-parallel to the electron beam direction.

The main systems required to realize DNP are the superconducting magnet to provide a strong (5 T) field, a ^{4}He evaporation refrigerator to maintain the target material at 1 K, a target insert, which will house the target material and some additional instrumentation, a microwave system to transfer the polarization to the nucleon spins, and a Nuclear Magnetic Resonance (NMR) system to determine the state of polarization.

In CLAS12 the polarizing magnetic field will be provided by the superconducting solenoid of the central detector. Ammonia and deuterated ammonia will be used as target material with the electron beam and CLAS12. In order to determine the dilution factor (fraction of events originating from unpolarized target materials) for each process with sufficiently high accuracy, about 20% of the running time will be devoted to measurements with carbon, nitrogen, and helium. To determine the proton to deuteron and deuteron to carbon cross section ratios, we will need a few days of running with the same magnetic fields and target position as the present experiment, but with gas or liquid hydrogen and deuterium targets. We anticipate that this can be scheduled in conjunction with other planned experiments with CLAS12.

For measurements on polarized deuterium, we may choose to use ^{6}LiD or HD as the target material, rather than ND_3. Both targets provide a very substantially higher dilution factor, and therefore substantially smaller statistical and systematic errors, for a given target polarization and luminosity. In the case of ^{6}LiD, the good dilution factor arises through the assumption that ^{6}LiD can be regarded to first approximation as an unpolarized alpha particle bound with a polarized deuteron. The frozen spin HD target has been recently transferred to JLab for a program of photoproduction experiments. Planned tests will show if this target

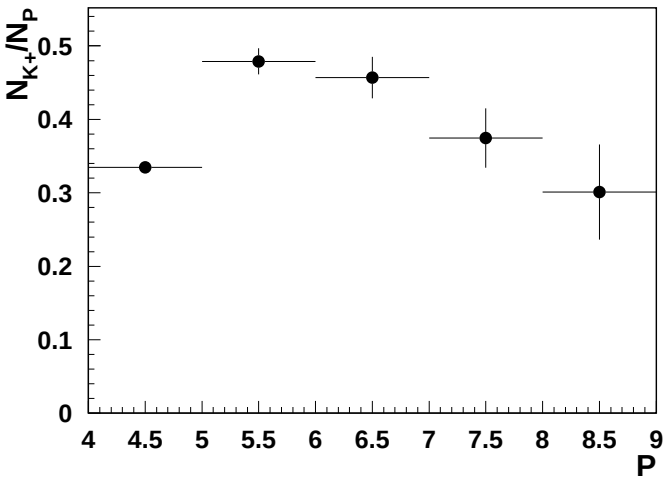

Figure 10: The ratio of K^+ to proton as a function of the momentum from CLAS12-DIS Monte-Carlo.

can withstand the heat load of a sufficiently high beam current to make this target material competitive with ND_3 or ^{6}LiD. If so, the very good dilution factor (over 50%) and lack of nuclear corrections from polarized nitrogen or lithium will make this the target of choice.

The target polarization will be monitored during the run via the NMR system, in the field of solenoid magnet. The calibration of the proton NMR can be done by measurements of polarization in thermal equilibrium, taken with the polarizing magnet.

2.3 The data set and analysis

The expected from the proposed experiment with 11 GeV beam and CLAS12 kinematic coverage in the DIS region is shown in Fig.12. This will constitute a substantial increase over the existing Jefferson Lab data in both x and Q^2 (maximum Q^2 of 5 GeV^2 and x between 0.2 and 0.6), while the precision of the expected data will be far superior to existing DIS experiments from other labs.

2.3.1 The polarized data set and analysis

The experiment will run with a beam of about 10 nA on a 3 cm long ammonia target, resulting in a luminosity of 10^{35}/cm^{2}s. The beam will be rastered over the diameter of the polarized target (about 3 cm) to minimize the dose density (we will need at most one anneal every other day under these conditions). We assume a beam polarization of 0.85, which has been routinely achieved in recent experiments running at Jefferson Lab. The beam helicity will be flipped in a pseudo-random pattern every 33 ms. We will use the standard Hall B beam devices to monitor and stabilize the beam intensity and position. In particular, we

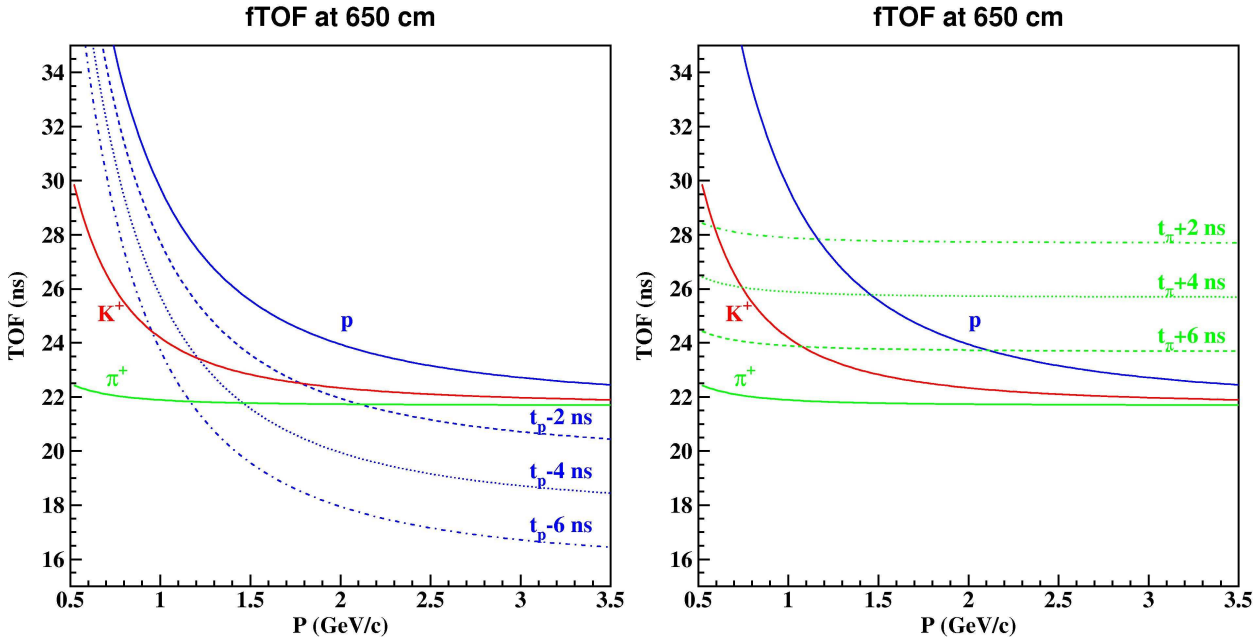

Figure 11: Time-of-flight of π^+s (green lines), K^+s (red lines), and protons (blue lines) from the target to the FTOF plane as a function momenta. On the left (right) graph - dashed line, dotted line, and dashed-dotted line correspond to protons (pions) from previous (next) beam buckets leaking into kaon samples

will reduce any helicity-correlated beam asymmetries to less than 10^{-3}.

The first-level trigger will consist of a coincidence between the high-threshold Cerenkov counter and a signal above threshold (corresponding to at least 1 GeV deposited) in the electromagnetic calorimeter in the same sector. This trigger will be highly specific for high-energy electrons, with little contamination from pions and other particles. In the case of too high background, we can also implement a level 2 trigger, which requires a electron candidate track in the drift chambers of the same sector as the level 1 trigger. This has already been developed for the present CLAS. The total event rate in the DIS region for this experiment is expected to be around 2000 Hz above $Q^2 = 1$ GeV^2. Estimated total maximal trigger rates that DAQ can handle are around 20 kHz. A data acquisition rate of 10 kHz has already been achieved with today's technology for the present CLAS DAQ. So that the required data acquisition rate for this experiment is a rather modest.

The data will consist of the number of counts for beam helicity anti-parallel (N^+) and parallel (N^-) to the longitudinal target polarization, each normalized to the dead-time corrected integrated beam charge. We will subtract from these rates the backgrounds from misidentified kaons (which can be obtained from fits to the distribution of photo-electrons in the high-threshold Cerenkov counter and the measured ratio of visible energy deposited in the electromagnetic calorimeter to the measured momentum) and from electrons coming from pair-symmetric decays (e.g., $\pi^0 \to e^+e^-$ or $\pi^0 \to \gamma e^+e^-$ as well as $\gamma \to e^+e^-$ conversions). From the corrected counts, we will form the ratio $A_{||}^{raw} = (N^+ - N^-)/(N^+ + N^-)$. This ratio has to be divided by the product of beam and target polarization and the dilution factor (the fraction of counts coming from the polarized nuclei in the target to the total).

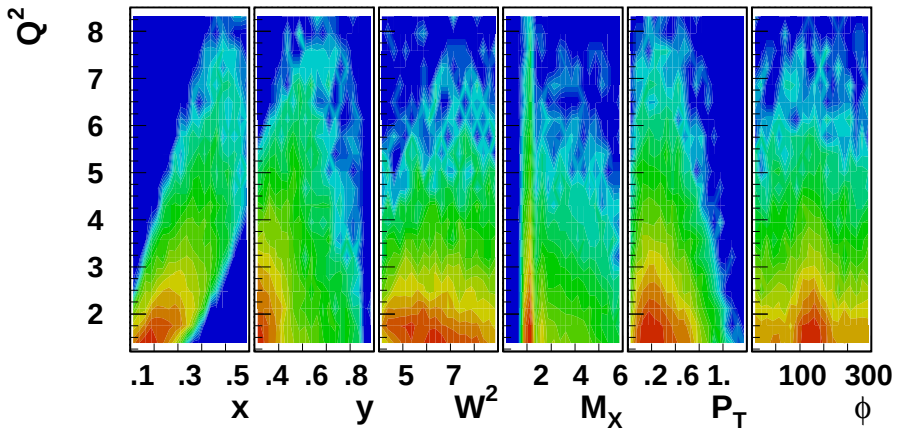

Figure 12: Kinematical coverage in the SIDIS region of the proposed experiment for eKX events.

The dilution factor can be calculated from a detailed model of the target content and a parametrization of the world data on unpolarized structure function for nucleons and nuclei (^{15}N, ^{4}He, and C and Al foils) in the target, including radiative effects. The only ingredient needed is the packing fraction (the fraction of the cell volume occupied by the ammonia beads), which can be extracted by comparing the rate from ammonia to that from an auxiliary carbon target. Additional measurements on empty and liquid-helium only targets will also be needed. Past experience with the EG1 experiment in Hall B has shown that a typical error of 3% on the dilution factor can be achieved [103]. An additional correction for the small polarization in ^{15}N and contamination by ^{14}N and, in the case of the deuterated ammonia, H, will be applied as well.

2.3.2 Azimuthal asymmetries

The beam (P_B) and target (P_T) polarization will be independently measured using Möller scattering and NMR, respectively. However, we can extract the product $P_B * P_T$ with higher precision directly from our data, by measuring the asymmetry of elastic (quasi-elastic) scattering $\vec{p}(\vec{e}, e'p)$ ($\vec{d}(\vec{e}, e'p)$) from our NH_3 (ND_3) targets, respectively. We did a full simulation of this method, including radiative effects, CLAS12 acceptance, and expected beam parameters. We find that the uncertainty on $P_B * P_T$ for the proton will be about 1% and on the

deuteron about 3%.

Measurements of average moments $\langle W(\phi)\rangle_{UL} = \int \sigma_{UL}(\phi)W(\phi)d\phi / \int \sigma(\phi)\sin^2\phi d\phi$ ($W(\phi) = \sin\phi, \sin 2\phi$) of the cross section $\sigma_{UL}^{W(\phi)}$ will single out corresponding terms in the cross section. Thus the $\sin\phi$ SSA of the cross section for longitudinally polarized target and unpolarized beam is defined as:

$$A_{UL}^{\sin\phi} = \frac{\langle \sin\phi\rangle_{UL}}{\langle \sin^2\phi\rangle_{UU}} = \frac{1}{P^{\pm}N^{\pm}} \frac{\sum_{i=1}^{N^{\pm}} \sin\phi_i}{\sum_{i=1}^{N^{\pm}} \sin^2\phi_i},$$

where $P^{\pm}$ and $N^{\pm}$ are the polarization and number of events for $\pm$ helicity state, respectively. For spin-dependent moments this is equivalent to the corresponding spin asymmetries A_{UL}^{W}. The final asymmetry is defined by the weighted average over two independent measurements for both helicity states or by fitting with corresponding azimuthal dependences ($\sin\phi, \sin 2\phi$) the spin asymmetries binned in the azimuthal angle.

2.3.3 Flavor decomposition and helicity distributions

The double spin asymmetry in SIDIS for charged and neutral hadrons is sensitive to the polarized parton densities through the different flavor sensitivities tagged by the hadron charge.

In terms of improved parton densities, an important observation is that the systematic errors largely cancel in the ratio of g_1/F_1 for SIDIS hadron production to the values for inclusive production. Therefore the ratios from Eqs 32-34, can be measured with high statistical and systematic precision (for example with relative errors of 3% in 2 bins in x). The depolarization factor D depends on the ratio R of longitudinal to transverse photo absorption cross sections, which is well known after a series of detailed experiments in Jefferson Lab's Hall C [104].

3 Expected results

3.1 Simulation

Realistic MC simulations were used for acceptance and efficiency studies as well as for understanding of radiative corrections [105, 106] and separation of different contributions to azimuthal moments arising also from higher twists. The CLAS12 FAST-MC program was used to simulate the physics events and study the extraction of azimuthal moments and acceptance corrections.

The expected number of counts and corresponding statistical errors in the following sections are based on a full simulation of inclusive and semi-inclusive inelastic scattering with the CLAS12 acceptance folded in. Events were generated with the clas12DIS generator [107]. This generator is basically an implementation of the LUND Monte Carlo package called PEPSI (Polarized Electron-Proton Scattering Interactions) [108]. It is based on polarized and unpolarized parton distribution functions and the LUND string model for hadronization, and has been tested successfully against several low-Q^2 experiments with 5.7 GeV beam at Jefferson Lab.

A fast Monte Carlo simulation program has been used to define the acceptance and resolution of the CLAS12 detector with all of the standard (base) equipment in place. The kaons were assumed identified 100% in sectors covered by CLAS12-RICH, and also at energies above 5 GeV, where the pions start to fire the High Threshold Cherekov Counter (HTCC). The events generated by clas12DIS are used as input and all particles are followed through all detector elements. The results of our simulation have been cross-checked with direct cross section calculations and a simple geometric acceptance model.

The resolution of the detector is simulated by a simple smearing function which modifies a particle's track by a random amount in momentum and angles according to a Gaussian distribution of the appropriate width. The amount of smearing follows the design specifications of the CLAS12 detector. The resolution in x_B varies between $0.01 < \sigma_x < 0.035$ and is therefore finer than our planned x bin size of 0.05 in all cases.

A full Monte Carlo simulation (GEANT-based) of CLAS12 with all resolution effects will be used to determine the effective mean x (and Q^2) for each x-bin we will use to bin our data so we can accurately extract the x-dependence of the measured asymmetries.

3.2 Statistical and systematic errors

The proposed spin asymmetry measurement is rather insensitive to uncertainties in acceptances and charge normalization. The overall statistics of kaons is, though, an order of magnitude less than for pions, with most of the relevant sources of systematic errors being the same. One of the main systematic error affecting the extraction of the Collins moment is due to possible contamination of the single kaon sample with kaons from decays of exclusive K^* mesons. The fraction of indirect kaons, however, according to LUND studies is significantly less than for pions (see Fig.13)

Other sources of systematic errors include the beam and target polarizations, dilution factor the longitudinal to transverse photo absorption cross section ratio, $R(x, Q^2)$. The main sources of systematic errors in measurements of single and double spin asymmetries

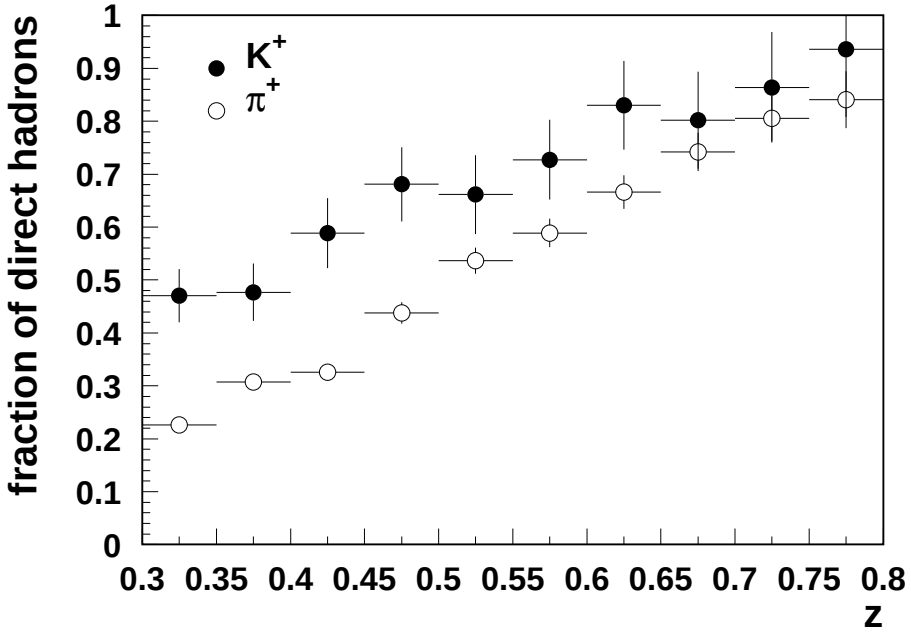

Figure 13: Fractions of direct (with a parent defined as "string") kaons and pions from PEPSI MC for ehX events.

are listed in the Table 5. These errors are all scale errors, so they are proportional to the size of the measured asymmetry. The total uncertainty is expected to be less than 10% of the measured SSA. For the $\sin 2\phi$ SSA, statistical uncertainties are expected to dominate the total uncertainty.

Studies of other sources of systematics, related to physics background, including target fragmentation, semi-exclusive processes, exclusive vector meson contributions, and higher twist require the data of this measurement.

We based our predicted statistical errors in the following sections on the assumption of running 30 days on NH_3 and 50 days on ND_3. The number of days was chosen to achieve a statistical error that is not significantly larger than the systematical error at the highest x and P_T points. More days on deuterium than the proton ensures that both have the same statistical error at large P_T and optimizes the error on extracted quantities like $h_{1L}^{\perp u,d}$ and $H_1^{\perp u/K^+}$.

For our estimate of the total systematic error, we have added the systematic errors from the various contributions discussed in the previous Section in quadrature. They are listed in Table 5. Note that some systematic errors (like the overall scale error coming from the beam and target polarization) affect the extraction of PDFs or higher twist contributions less than point-to-point errors, which typically are smaller. Additional contributions to systematic error of measured asymmetries will come from uncertainties of unpolarized structure

Table 5: Uncertainties for asymmetry measurements.

Item	A_1^p	$A_{UL}^{\sin\phi}$	$A_{UL}^{\sin 2\phi}$
beam x target polarization	2%	-	-
target polarization	-	3%	3%
depolarization and R	4%	-	-
dilution factor	3%	3%	3%
radiative corrections	3%	3%	3%
fitting procedure	-	4%	5%
transverse (to γ^*) spin effects	3%	3%	-%

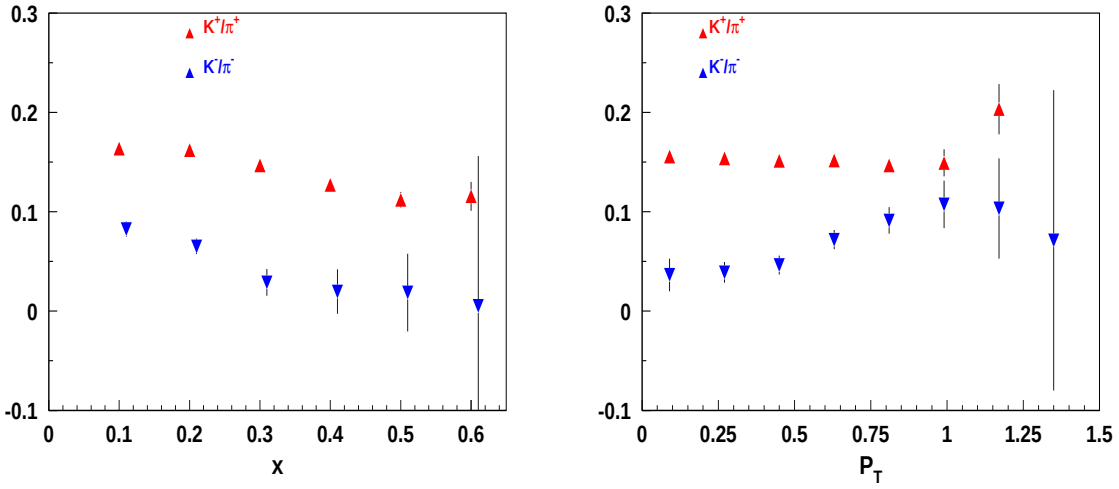

(a) (b)

Figure 14: PEPSI-Lepto predictions for x-dependence (left) and P_T-dependence of kaon pion ratios.

functions and also attenuation of hadrons in nuclear environment, which are a subject of a separate study (PAC-30 proposal on nuclei).

3.3 Results

The proposed experiment will simultaneously collect data on $\vec{p}, \vec{d}(\vec{e}, e'h)$, including kaons and pions. The charged kaons will be detected in the forward spectrometer and the central tracker of CLAS12 in coincidence with the scattered electrons and identified by the CLAS12-RICH detector. The following predicted results were obtained with a full simulation of the hadronization process [108] and the acceptance of CLAS12 for all particles.

The expected counts of kaons in different kinematic bins for the hydrogen and deuteron targets for each of the kaon charges were calculated using the PEPSI-MC kaon to pion ratios (Fig.14).

The main difference from the pion production case for the background, is the contribution

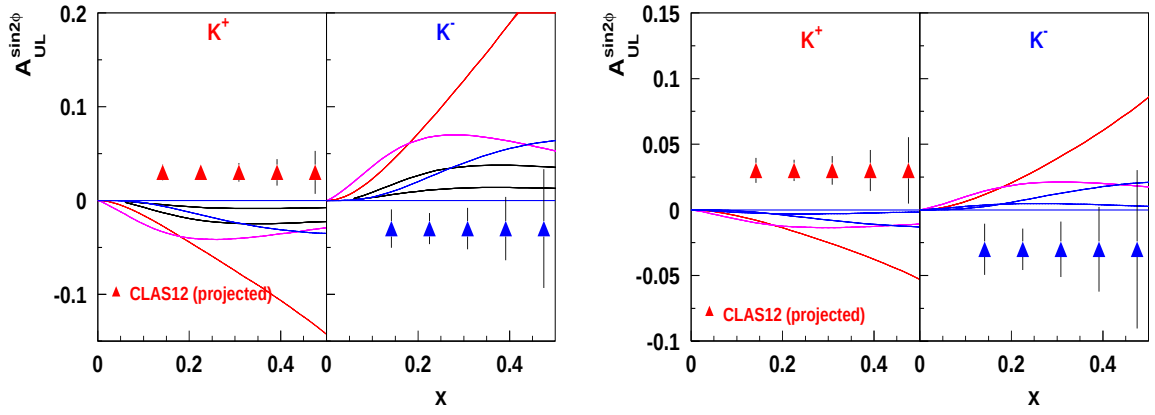

Figure 15: The projected x-dependence of the target SSA at 11 GeV for proton (left) and deuteron (right) targets. The triangles illustrate the expected statistical accuracy. The black curves show the bounds for calculations based on the relations between transversity and $h_{1L}^{\perp}$ [83]. Color curves correspond to calculations in constituent quark model [88] using different wave functions.

from diffractive K^* production (e.g., $K^* \to K\pi$) and the radiative tail on exclusive Kaon production. The contributions to the systematic error from these backgrounds requires a detailed analysis once the requisite data are in hand, but experience with pion data from CLAS at 6 GeV show that one can avoid most of them by judicious choice of kinematic cuts.

3.3.1 Projected results with polarized target running

Projections for the resulting kinematic dependence of the leading-twist SSA are shown in Fig. 15. Calculations were done using $h_{1L}^{\perp}$ from the chiral quark soliton model evolved to Q^2=1.5 GeV^2 [47], f_1 from GRV95 [90], and D_1 from Kretzer, Leader, and Christova [91]. Corresponding projected error bars for the RSMT TMD parton distribution are shown in Fig. 15. The black curves are calculated assuming the so-called "Lorentz-invariance relations" that connect $h_{1L}^{\perp}$ with h_1 [2]. This measurement will check out experimentally to which extent such relations actually hold [65, 64]. The read and blue curves are calculations in constituent quark model [88] using Schlumpf's wave function [109] and the hypercentral wave function for the momentum dependence of the light-cone wave function [110]. Both wave functions were used assuming no evolution of $h_{1L}^{\perp}$ and by evolving $h_{1L}^{\perp}$ in the same way as the transversity In both cases, in the denominator the unpolarized PDF f_1 from GRV98 was used, evolved at $Q^2 = 2.5 GeV^2$.

Proposed measurements of SSAs in SIDIS will measure the ratio of favored to unfavored polarized fragmentation functions for kaons provide independent to pion measurements constrains on the corresponding TMD distributions. The new data will also allow a more precise test of the factorization ansatz and the investigation of the Q^2 dependence of $\sin 2\phi$, $\sin \phi$, and $\cos \phi$ asymmetries. This will enable us to study the leading-twist and higher-twist nature

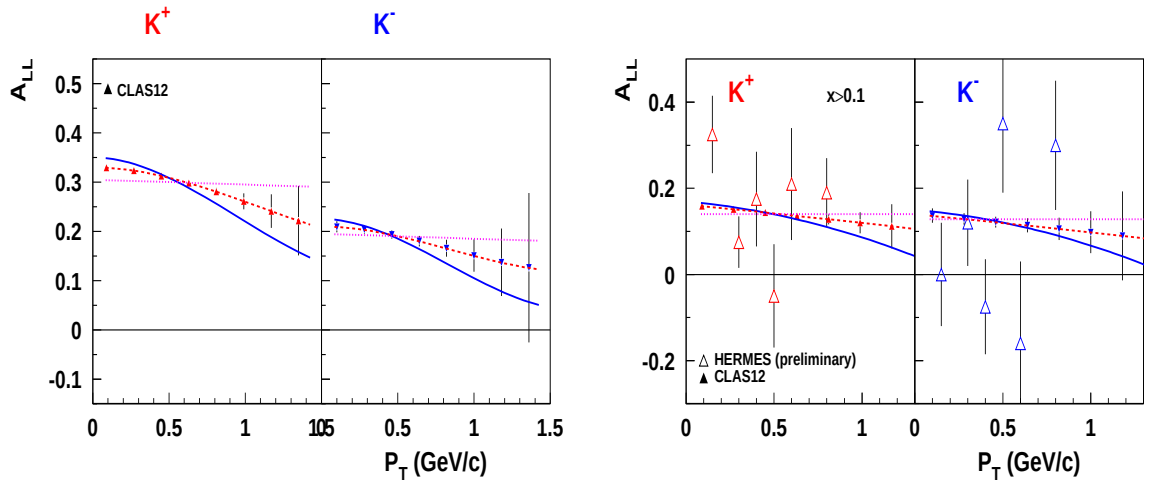

(a) (b)

Figure 16: The double spin asymmetry A_{LL} for the NH_3-target (left) and ND_3-target (right) as a function of the transverse momentum of hadrons, P_T, averaged in the $0.4 < z < 0.7$ range. Curves are calculated using different k_T widths for helicity distributions [37].

of the corresponding observables [111, 78, 112, 59, 60, 61, 13].

Measurement of the P_T dependence of the Kotzinian-Mulders-asymmetry will also allow for checking of the high P_T predictions [12, 113, 45] to study the transition from a non-perturbative to a perturbative description. The $\sin 2\phi$ asymmetry in the kinematic region of CLAS12 is predicted to be significant (a few percent on average) and tending to be larger in the large-x and large-z region.

The combined analysis of the future CLAS12 data on $\langle \sin 2\phi \rangle$ and of the previous HERMES measurements in the high-Q^2 domain (where higher-twist effects are less significant) will provide information on the RSMT function, shedding light on the correlations between transverse spin and transverse momenta of quarks. Significantly increasing the kinematic coverage at large Q^2 and P_T, CLAS12 (see Fig. 15) will map the quark TMDs in the valence region allowing study of the transition from a non-perturbative description at small P_T to a perturbative description at large P_T.

At lower x, this very large data set allows us to further subdivide the data into bins in P_T and z. Once in hand, these data will be combined with CLAS12 data on pions and existing SIDIS data from HERMES, COMPASS and RHIC for a full NLO analysis.

Projections for the resulting P_T-dependence of the double spin asymmetries for charged kaons are shown in for NH_3 and ND_3 targets in Fig. 16. These measurements using unfolding of Eqs.28-29 would be complementary to pion asymmetries, accessing the k_T-distributions of u and d-quarks aligned and anti-aligned with the spin of the nucleon. Integrated over the transverse momentum the data will also be used for consistency checking of the k_T-integrated standard PDFs, which are the subject of a different proposal [114].

Measured single and double spin asymmetries for kaons in a large range of kinematic variables (x_B, Q^2, z, $P_\perp$ and ϕ) combined with measurements with unpolarized target mea-

surements and data for pions [39], will provide detailed information on flavor and polarization dependence of transverse momentum distributions of quarks in valence region and in particular on the x_B and k_T dependence of leading TMD parton distribution functions. Measurements of spin and azimuthal asymmetries across a wide range of x, z, Q^2, and P_T would allow to perform detailed tests of QCD dynamics in valence region.

Time	Activity
3 days	Commissioning: Beam raster set up, trigger optimization, low energy calibration runs
30 days	Production data taking on NH_3
50 days	Production data taking on ND_3
3 days (1 1/2 hours every other day)	Target anneals and/or target changes
10 days (intermittent with production data)	Calibration runs on ^{12}C and empty target
5 days	Production runs on ^{15}N
2 day (1 hour every other day – concurrent with anneals)	Möller polarimeter runs

Table 6: Requested beam time broken down by activity.

4 Summary and Request

Understanding of spin-orbit correlations, together with independent measurements related to the spin and orbital angular momentum of the quarks, will help to construct a more complete picture of the nucleon in terms of elementary quarks and gluons going beyond the simple collinear partonic representation. The proposed set of measurements with longitudinally polarized proton and deuteron targets will yield a comprehensive set of azimuthal moments in spin-dependent and independent SIDIS providing access to corresponding distribution and fragmentation functions in a wide range of x, Q^2, z, and P_T. Our data, combined with the data from HERMES, COMPASS, and BELLE, will provide independent (complementary to $e+/e-$) measurement of polarized kaon Collins fragmentation function and will allow a complementary to pion SIDIS study of leading twist TMD parton distributions $g_1(x, k_T)$ and $h_{1L}^{\perp}(x, k_T)$. In addition, the proposed experiment will yield data on single (target and beam) spin asymmetries in SIDIS, which can provide constraints on the higher-twist nucleon structure functions and provide complementary to transverse target information on spin-orbit correlations (the LOI submitted to PAC-34 [115]).

To achieve this goal, we request a total of 103 days of beam time with an 11 GeV, 10 nA highly polarized electron beam in Hall B. The breakdown of this beam time is shown in Table 6.

We want to conclude by noting that while this proposed experiments requires a substantial commitment of beam time (103 days total), we will simultaneously take data with already approved experiments to study the inclusive and semi-inclusive DIS [97, 39].

Appendix-I

Isospin and charge-conjugation relations imply for "favored" functions

$$D_1^{u\to\pi^+} = D_1^{\bar{d}\to\pi^+} = D_1^{d\to\pi^-} = D_1^{\bar{u}\to\pi^-}, \equiv D_1^{\rm f} \tag{36}$$

$$D_1^{u\to K^+} = D_1^{\bar{u}\to K^-}, \equiv D_1^{\rm fd} \tag{37}$$

$$D_1^{\bar{s}\to K^+} = D_1^{s\to K^-} \equiv D_1^{\rm f'} \tag{38}$$

for the "unfavored" functions

$$D_1^{\bar{u}\to\pi^+} = D_1^{d\to\pi^+} = D_1^{\bar{d}\to\pi^-} = D_1^{u\to\pi^-} \equiv D_1^{\rm d}, \tag{39}$$

$$D_1^{s\to\pi^+} = D_1^{\bar{s}\to\pi^+} = D_1^{s\to\pi^-} = D_1^{\bar{s}\to\pi^-} \equiv D_1^{\rm df}, \tag{40}$$

$$D_1^{\bar{u}\to K^+} = D_1^{\bar{d}\to K^+} = D_1^{d\to K^+} = D_1^{\bar{d}\to K^-} = D_1^{d\to K^-} = D_1^{u\to K^-} \equiv D_1^{\rm dd}, \tag{41}$$

$$D_1^{s\to K^+} = D_1^{\bar{s}\to K^-} \equiv D_1^{\rm d'}. \tag{42}$$

There are in principle seven independent functions. Further assumption could be to set $D_1^{\rm f'} = D_1^{\rm f}$ and $D_1^{\rm d'} = D_1^{\rm d}$, leaving five independent functions.

For the Collins function, one can consider the Schäfer–Teryaev sum rule [116], which states that

$$\sum_h \int_0^1 dz H_{1(q\to h)}^{\perp(1)}(z) = 0 \qquad \text{with} \qquad H_1^{\perp(1)}(z) = \pi z^2 \int_0^\infty dk_T^2 \, \frac{\boldsymbol{k}_T^2}{2M_h^2} \, H_1^\perp(z, k_T^2). \tag{43}$$

Assuming that the sum rule holds in a strong sense, i.e., for pions and kaons separately and at the integrand level, for each value of z and k_T. For pions, using also it follows that

$$H_{1(u\to\pi^+)}^\perp = H_{1(\bar{d}\to\pi^+)}^\perp = H_{1(d\to\pi^-)}^\perp = H_{1(\bar{u}\to\pi^-)}^\perp \equiv H_1^{\perp\rm f} \tag{44}$$

$$H_{1(u\to\pi^-)}^\perp = H_{1(d\to\pi^+)}^\perp = H_{1(d\to\pi^+)}^\perp = H_{1(\bar{u}\to\pi^+)}^\perp \equiv -H_1^{\perp\rm f} \tag{45}$$

With such a "strong" interpretation of the Schäfer–Teryaev sum rule together with Eq. (40) (with D_1 replaced by $H_1^\perp$) implies

$$H_{1(s\to\pi^+)}^\perp = -H_{1(s\to\pi^-)}^\perp = H_{1(\bar{s}\to\pi^+)}^\perp = -H_{1(\bar{s}\to\pi^-)}^\perp = 0. \tag{46}$$

For kaons, the same considerations lead to the following assumptions

$$H_{1(u\to K^+)}^\perp = H_{1(\bar{u}\to K^-)}^\perp \equiv H_1^{\perp\rm fd}, \tag{47}$$

$$H_{1(u\to K^-)}^\perp = H_{1(\bar{u}\to K^+)}^\perp \equiv -H_1^{\perp\rm fd}, \tag{48}$$

$$H_{1(\bar{s}\to K^+)}^\perp = H_{1(s\to K^-)}^\perp \equiv H_1^{\perp\rm f'}, \tag{49}$$

$$H_{1(\bar{s}\to K^-)}^\perp = H_{1(s\to K^+)}^\perp \equiv -H_1^{\perp\rm f'}, \tag{50}$$

$$H_{1(d\to K^-)}^\perp = -H_{1(d\to K^+)}^\perp = H_{1(\bar{d}\to K^-)}^\perp = -H_{1(\bar{d}\to K^+)}^\perp = 0. \tag{51}$$

In total, we are left with only three independent Collins functions.

Then pion and kaon *weighted* asymmetries can be written as (using a generic chiral-odd function as an example)

$$A^{p/\pi^+}(x,y,z) = \frac{B(y)}{A(y)} \frac{\left(4\,h^u + h^{\bar{d}}\right) H_1^{\perp(1)\mathrm{f}} - \left(4\,h^{\bar{u}} + h^d\right) H_1^{\perp(1)\mathrm{f}}}{\left(4\,f_1^u + f_1^{\bar{d}}\right) D_1^{\mathrm{f}} + \left(4\,f_1^{\bar{u}} + f_1^d\right) D_1^{\mathrm{d}} + \left(f_1^s + f_1^{\bar{s}}\right) D_1^{\mathrm{df}}}, \tag{52}$$

$$A^{p/\pi^-}(x,y,z) = \frac{B(y)}{A(y)} \frac{\left(4\,h^{\bar{u}} + h^d\right) H_1^{\perp(1)\mathrm{f}} - \left(4\,h^u + h^{\bar{d}}\right) H_1^{\perp(1)\mathrm{f}}}{\left(4\,f_1^{\bar{u}} + f_1^d\right) D_1^{\mathrm{f}} + \left(4\,f_1^u + f_1^{\bar{d}}\right) D_1^{\mathrm{d}} + \left(f_1^s + f_1^{\bar{s}}\right) D_1^{\mathrm{df}}}, \tag{53}$$

$$A^{n/\pi^+}(x,y,z) = \frac{B(y)}{A(y)} \frac{\left(4\,h^d + h^{\bar{u}}\right) H_1^{\perp(1)\mathrm{f}} - \left(4\,h^{\bar{d}} + h^u\right) H_1^{\perp(1)\mathrm{f}}}{\left(4\,f_1^d + f_1^{\bar{u}}\right) D_1^{\mathrm{f}} + \left(4\,f_1^{\bar{d}} + f_1^u\right) D_1^{\mathrm{d}} + \left(f_1^s + f_1^{\bar{s}}\right) D_1^{\mathrm{df}}}, \tag{54}$$

$$A^{n/\pi^-}(x,y,z) = \frac{B(y)}{A(y)} \frac{\left(4\,h^{\bar{d}} + h^u\right) H_1^{\perp(1)\mathrm{f}} - \left(4\,h^d + h^{\bar{u}}\right) H_1^{\perp(1)\mathrm{f}}}{\left(4\,f_1^{\bar{d}} + f_1^u\right) D_1^{\mathrm{f}} + \left(4\,f_1^d + f_1^{\bar{u}}\right) D_1^{\mathrm{d}} + \left(f_1^s + f_1^{\bar{s}}\right) D_1^{\mathrm{df}}}, \tag{55}$$

$$A^{p/K^+}(x,y,z) = \frac{B(y)}{A(y)} \frac{4\left(h^u - h^{\bar{u}}\right) H_1^{\perp(1)\mathrm{fd}} - \left(h^s - h^{\bar{s}}\right) H_1^{\perp(1)\mathrm{f}'}}{4\,f_1^u\,D_1^{\mathrm{fd}} + \left(4\,f_1^{\bar{u}} + f_1^d + f_1^{\bar{d}}\right) D_1^{\mathrm{dd}} + f_1^{\bar{s}}\,D_1^{\mathrm{f}'} + f_1^s\,D_1^{\mathrm{d}'}}, \tag{56}$$

$$A^{p/K^-}(x,y,z) = \frac{B(y)}{A(y)} \frac{-4\left(h^u - h^{\bar{u}}\right) H_1^{\perp(1)\mathrm{fd}} + \left(h^s - h^{\bar{s}}\right) H_1^{\perp(1)\mathrm{f}'}}{4\,f_1^{\bar{u}}\,D_1^{\mathrm{fd}} + \left(4\,f_1^u + f_1^d + f_1^{\bar{d}}\right) D_1^{\mathrm{dd}} + f_1^s\,D_1^{\mathrm{f}'} + f_1^{\bar{s}}\,D_1^{\mathrm{d}'}}, \tag{57}$$

$$A^{n/K^+}(x,y,z) = \frac{B(y)}{A(y)} \frac{4\left(h^d - h^{\bar{d}}\right) H_1^{\perp(1)\mathrm{fd}} - \left(h^s - h^{\bar{s}}\right) H_1^{\perp(1)\mathrm{f}'}}{4\,f_1^d\,D_1^{\mathrm{fd}} + \left(4\,f_1^{\bar{d}} + f_1^u + f_1^{\bar{u}}\right) D_1^{\mathrm{dd}} + f_1^{\bar{s}}\,D_1^{\mathrm{f}'} + f_1^s\,D_1^{\mathrm{d}'}}, \tag{58}$$

$$A^{n/K^-}(x,y,z) = \frac{B(y)}{A(y)} \frac{-4\left(h^d - h^{\bar{d}}\right) H_1^{\perp(1)\mathrm{fd}} + \left(h^s - h^{\bar{s}}\right) H_1^{\perp(1)\mathrm{f}'}}{4\,f_1^{\bar{d}}\,D_1^{\mathrm{fd}} + \left(4\,f_1^d + f_1^u + f_1^{\bar{u}}\right) D_1^{\mathrm{dd}} + f_1^s\,D_1^{\mathrm{f}'} + f_1^{\bar{s}}\,D_1^{\mathrm{d}'}}, \tag{59}$$

The sums of the numerators of the π^+ and π^- and of the K^+ and K^- observables always vanish.

Appendix-II: Subleading-twist azimuthal and spin asymmetries

Assuming factorization, subleading-twist azimuthal moments are given in a tree-level formalism in terms of twist-3 TMDs. More precisely, they are due to the following structure

functions (in the notation of [3]):

$$F_{UU}^{\cos\phi_h} = \frac{2M}{Q}\,\mathcal{C}\left[-\frac{\mathbf{h}_\perp \mathbf{k}_T}{m_h}\left(xh\,H_1^\perp + \frac{m_h}{M}\,f_1\frac{\tilde{D}^\perp}{z}\right) - \frac{\mathbf{h}_\perp \mathbf{p}_T}{M}\left(xf^\perp D_1 + \frac{m_h}{M}\,h_1^\perp\frac{\tilde{H}}{z}\right)\right], \quad (60)$$

$$F_{UL}^{\sin\phi_h} = \frac{2M}{Q}\,\mathcal{C}\left[-\frac{\mathbf{h}_\perp \mathbf{k}_T}{m_h}\left(xh_L H_1^\perp + \frac{m_h}{M}\,g_1\frac{\tilde{G}^\perp}{z}\right) + \frac{\mathbf{h}_\perp \mathbf{p}_T}{M}\left(xf_L^\perp D_1 - \frac{m_h}{M}\,h_{1L}^\perp\frac{\tilde{H}}{z}\right)\right], \quad (61)$$

$$F_{LU}^{\sin\phi_h} = \frac{2M}{Q}\,\mathcal{C}\left[-\frac{\mathbf{h}_\perp \mathbf{k}_T}{m_h}\left(xe\,H_1^\perp + \frac{m_h}{M}\,f_1\frac{\tilde{G}^\perp}{z}\right) + \frac{\mathbf{h}_\perp \mathbf{p}_T}{M}\left(xg^\perp D_1 + \frac{m_h}{M}\,h_1^\perp\frac{\tilde{E}}{z}\right)\right], \quad (62)$$

$$F_{LL}^{\cos\phi_h} = \frac{2M}{Q}\,\mathcal{C}\left[\frac{\mathbf{h}_\perp \mathbf{k}_T}{m_h}\left(xe_L H_1^\perp - \frac{m_h}{M}\,g_1\frac{\tilde{D}^\perp}{z}\right) - \frac{\mathbf{h}_\perp \mathbf{p}_T}{M}\left(xg_L^\perp D_1 + \frac{m_h}{M}\,h_{1L}^\perp\frac{\tilde{E}}{z}\right)\right], \quad (63)$$

References

[1] European Muon, J. Ashman et al., Phys. Lett. B206 (1988) 364.

[2] P.J. Mulders and R.D. Tangerman, Nucl. Phys. B461 (1996) 197, hep-ph/9510301.

[3] A. Bacchetta et al., JHEP 02 (2007) 093, hep-ph/0611265.

[4] V. Barone, A. Drago and P.G. Ratcliffe, Phys. Rept. 359 (2002) 1, hep-ph/0104283.

[5] D.W. Sivers, Phys. Rev. D43 (1991) 261.

[6] M. Anselmino and F. Murgia, Phys. Lett. B442 (1998) 470, hep-ph/9808426.

[7] S.J. Brodsky, D.S. Hwang and I. Schmidt, Phys. Lett. B530 (2002) 99, hep-ph/0201296.

[8] J.C. Collins, Phys. Lett. B536 (2002) 43, hep-ph/0204004.

[9] X. Ji and F. Yuan, Phys. Lett. B543 (2002) 66, hep-ph/0206057.

[10] A.V. Belitsky, X. Ji and F. Yuan, Nucl. Phys. B656 (2003) 165, hep-ph/0208038.

[11] D. Boer, P.J. Mulders and F. Pijlman, Nucl. Phys. B667 (2003) 201, hep-ph/0303034.

[12] X. Ji, J. Ma and F. Yuan, Phys. Rev. D71 (2005) 034005, hep-ph/0404183.

[13] J.C. Collins and A. Metz, Phys. Rev. Lett. 93 (2004) 252001, hep-ph/0408249.

[14] X.d. Ji, J.P. Ma and F. Yuan, Nucl. Phys. B652 (2003) 383, hep-ph/0210430.

[15] S.J. Brodsky, D.S. Hwang and I. Schmidt, Nucl. Phys. B642 (2002) 344, hep-ph/0206259.

[16] J.P. Ralston and D.E. Soper, Nucl. Phys. B152 (1979) 109.

[17] C.J. Bomhof and P.J. Mulders, Nucl. Phys. B795 (2008) 409.

[18] J. Collins and J.W. Qiu, Phys. Rev. D75 (2007) 114014, 0705.2141.

[19] W. Vogelsang and F. Yuan, Phys. Rev. D76 (2007) 094013, 0708.4398.

[20] J.C. Collins, Nucl. Phys. B396 (1993) 161, hep-ph/9208213.

[21] A. Metz, Phys. Lett. B549 (2002) 139.

[22] F. Yuan, Phys. Rev. D77 (2008) 074019, 0801.3441.

[23] HERMES, A. Airapetian et al., Phys. Rev. Lett. 84 (2000) 4047, hep-ex/9910062.

[24] HERMES, A. Airapetian et al., Phys. Rev. D64 (2001) 097101, hep-ex/0104005.

[25] HERMES, A. Airapetian et al., Phys. Rev. Lett. 94 (2005) 012002, hep-ex/0408013.

[26] HERMES, A. Airapetian, (2006), hep-ex/0612059.

[27] COMPASS, V.Y. Alexakhin et al., Phys. Rev. Lett. 94 (2005) 202002, hep-ex/0503002.

[28] CLAS, H. Avakian et al., Phys. Rev. D69 (2004) 112004, hep-ex/0301005.

[29] CLAS, H. Avakian et al., AIP Conf. Proc. 792 (2005) 945, nucl-ex/0509032.

[30] STAR, J. Adams et al., Phys. Rev. Lett. 92 (2004) 171801, hep-ex/0310058.

[31] PHENIX, M. Chiu, AIP Conf. Proc. 915 (2007) 539, nucl-ex/0701031.

[32] BRAHMS, I. Arsene et al., Phys. Rev. Lett. 101 (2008) 042001, 0801.1078.

[33] Belle, K. Abe et al., Phys. Rev. Lett. 96 (2006) 232002, hep-ex/0507063.

[34] H. Avakian et al., (2007), arXiv:0705.1553 [hep-ph].

[35] A. Bacchetta et al., (2008), 0807.0323.

[36] R. Jakob, P.J. Mulders and J. Rodrigues, (1997), hep-ph/9707340.

[37] M. Anselmino et al., Phys. Rev. D74 (2006) 074015, hep-ph/0608048.

[38] A.M. Kotzinian and P.J. Mulders, Phys. Rev. D54 (1996) 1229, hep-ph/9511420.

[39] H. Avakian et al., JLab Experiment E12-07-015 (2008).

[40] A. Kotzinian, Nucl. Phys. B441 (1995) 234, hep-ph/9412283.

[41] D. Boer and P.J. Mulders, Phys. Rev. D57 (1998) 5780, hep-ph/9711485.

[42] R.D. Tangerman and P.J. Mulders, Phys. Rev. D51 (1995) 3357, hep-ph/9403227.

[43] S.J. Brodsky and F. Yuan, Phys. Rev. D74 (2006) 094018, hep-ph/0610236.

[44] P.V. Pobylitsa, (2003), hep-ph/0301236.

[45] A. Bacchetta et al., JHEP 08 (2008) 023, 0803.0227.

[46] A. Bacchetta et al., Phys. Rev. Lett. 85 (2000) 712, hep-ph/9912490.

[47] A.V. Efremov, K. Goeke and P. Schweitzer, Phys. Rev. D67 (2003) 114014, hep-ph/0208124.

[48] M. Anselmino et al., (2007), hep-ph/0701006.

[49] A. Bacchetta et al., Phys. Lett. B659 (2008) 234, 0707.3372.

[50] HERMES, A. Airapetian et al., Phys. Rev. Lett. 84 (2000) 2584, hep-ex/9907020.

[51] Spin Muon (SMC), B. Adeva et al., Phys. Rev. D70 (2004) 012002, hep-ex/0402010.

[52] COMPASS, E.S. Ageev et al., Phys. Lett. B633 (2006) 25, hep-ex/0511028.

[53] PHENIX, A. Adare, (2007), arXiv:0704.3599 [hep-ex].

[54] European Muon, M. Arneodo et al., Z. Phys. C34 (1987) 277.

[55] HERMES, H. Avakian, Nucl. Phys. Proc. Suppl. 79 (1999) 523.

[56] HERMES, A. Airapetian et al., Phys. Lett. B562 (2003) 182, hep-ex/0212039.

[57] HERMES, A. Airapetian et al., Phys. Lett. B622 (2005) 14, hep-ex/0505042.

[58] CLAS, H. Avakian, (2008), PANIC-2008 proceedings.

[59] A. Afanasev and C.E. Carlson, (2003), hep-ph/0308163.

[60] F. Yuan, Phys. Lett. B589 (2004) 28, hep-ph/0310279.

[61] A. Metz and M. Schlegel, Eur. Phys. J. A22 (2004) 489, hep-ph/0403182.

[62] A. Metz and M. Schlegel, Annalen Phys. 13 (2004) 699, hep-ph/0411118.

[63] A. Bacchetta, P.J. Mulders and F. Pijlman, Phys. Lett. B595 (2004) 309, hep-ph/0405154.

[64] K. Goeke, A. Metz and M. Schlegel, Phys. Lett. B618 (2005) 90, hep-ph/0504130.

[65] K. Goeke et al., Phys. Lett. B567 (2003) 27, hep-ph/0302028.

[66] L.P. Gamberg et al., Phys. Lett. B639 (2006) 508, hep-ph/0604022.

[67] M. Burkardt, (2008), 0810.3589.

[68] E. De Sanctis, W.D. Nowak and K.A. Oganesian, Phys. Lett. B483 (2000) 69, hep-ph/0002091.

[69] K.A. Oganessian et al., Nucl. Phys. A689 (2001) 784, hep-ph/0010261.

[70] M. Anselmino and F. Murgia, Phys. Lett. B483 (2000) 74, hep-ph/0002120.

[71] A.V. Efremov, K. Goeke and P. Schweitzer, Phys. Lett. B522 (2001) 37, hep-ph/0108213.

[72] A.V. Efremov, K. Goeke and P. Schweitzer, Eur. Phys. J. C24 (2002) 407, hep-ph/0112166.

[73] A.V. Efremov, K. Goeke and P. Schweitzer, Phys. Lett. B568 (2003) 63, hep-ph/0303062.

[74] B.Q. Ma, I. Schmidt and J.J. Yang, Phys. Rev. D66 (2002) 094001, hep-ph/0209114.

[75] A.V. Efremov, K. Goeke and P. Schweitzer, Eur. Phys. J. C32 (2003) 337, hep-ph/0309209.

[76] K. Kramer et al., Phys. Rev. Lett. 95 (2005) 142002, nucl-ex/0506005.

[77] S. Wandzura and F. Wilczek, Phys. Lett. B72 (1977) 195.

[78] R.L. Jaffe and X.D. Ji, Nucl. Phys. B375 (1992) 527.

[79] R.L. Jaffe and X.D. Ji, Phys. Rev. Lett. 67 (1991) 552.

[80] B. Dressler and M.V. Polyakov, Phys. Rev. D61 (2000) 097501, hep-ph/9912376.

[81] K. Efremov, A. V. Goeke and P. Schweitzer, Private communication 08 (2003) 006, hep-ph/0212044.

[82] A.V. Efremov and P. Schweitzer, JHEP 08 (2003) 006, hep-ph/0212044.

[83] H. Avakian et al., Phys. Rev. D77 (2008) 014023, 0709.3253.

[84] A. Metz, P. Schweitzer and T. Teckentrup, (2008), 0810.5212.

[85] M. Anselmino et al., Phys. Rev. D71 (2005) 074006, hep-ph/0501196.

[86] J.C. Collins et al., Phys. Rev. D73 (2006) 014021, hep-ph/0509076.

[87] S. Boffi et al., (2008) in preparation.

[88] B. Pasquini, S. Cazzaniga and S. Boffi, Phys. Rev. D78 (2008) 034025, 0806.2298.

[89] H. Avakian et al., JLab Experiment E12-06-015 (2008).

[90] M. Gluck et al., Phys. Rev. D53 (1996) 4775, hep-ph/9508347.

[91] S. Kretzer, E. Leader and E. Christova, Eur. Phys. J. C22 (2001) 269, hep-ph/0108055.

[92] A.V. Efremov, K. Goeke and P. Schweitzer, Phys. Rev. D73 (2006) 094025, hep-ph/0603054.

[93] S.J. Brodsky and S.D. Drell, Phys. Rev. D22 (1980) 2236.

[94] S.J. Brodsky, M. Burkardt and I. Schmidt, Nucl. Phys. B441 (1995) 197, hep-ph/9401328.

[95] M. Gockeler et al., Nucl. Phys. Proc. Suppl. 153 (2006) 146, hep-lat/0512011.

[96] A.V. Efremov, K. Goeke and P. Schweitzer, Czech. J. Phys. 55 (2005) A189, hep-ph/0412420.

[97] Jefferson Lab Hall B, S. Kuhn et al., PAC30 Proposal (2006).

[98] F. Garibaldi et al., Nucl. Instrum. Meth. A502 (2003) 117.

[99] M. Iodice et al., Nucl. Instrum. Meth. A553 (2005) 231.

[100] Hall-A, F. Garibaldi et al., JLab Experiment E94-107 (1994).

[101] A.S. Group, CERN Program Library Long Writeup W501 WWW://wwwinfo.cern.ch/asdoc/*geant_html*3/geantall.html (2003).

[102] CLAS, P. Rossi et al., http://www.jlab.org/∼rossi/rich/*rich_v*2.pdf (2008).

[103] CLAS, K.V. Dharmawardane et al., Phys. Lett. B641 (2006) 11, nucl-ex/0605028.

[104] CLAS, P.E. Bosted et al., Phys. Rev. C78 (2008) 015202, 0712.2438.

[105] I. Akushevich, N. Shumeiko and A. Soroko, Eur. Phys. J. C10 (1999) 681, hep-ph/9903325.

[106] I. Akushevich, A. Ilyichev and M. Osipenko, (2007), 0711.4789.

[107] H. Avakian and P. Bosted., (2006).

[108] L. Mankiewicz, A. Schafer and M. Veltri, Comput. Phys. Commun. 71 (1992) 305.

[109] S.J. Brodsky and F. Schlumpf, Phys. Lett. B329 (1994) 111, hep-ph/9402214.

[110] P. Faccioli, M. Traini and V. Vento, Nucl. Phys. A656 (1999) 400, hep-ph/9808201.

[111] J. Levelt and P.J. Mulders, Phys. Lett. B338 (1994) 357, hep-ph/9408257.

[112] A.M. Kotzinian et al., (1999), hep-ph/9908466.

[113] X. Ji et al., Phys. Rev. D73 (2006) 094017, hep-ph/0604023.

[114] K. Hafidi et al., JLab Experiment E12-XX-XXX (2008).

[115] Jefferson Lab Hall B, . H.Avakian et al., LOI to PAC34 (2008).

[116] A. Schafer and O.V. Teryaev, Phys. Rev. D61 (2000) 077903, hep-ph/9908412.